Available online at www.sciencedirect.com
ScienceDirect
Comput. Methods Appl. Mech. Engrg. 338 (2018) 412–439
Computer methods in applied mechanics and engineering
www.elsevier.com/locate/cma

Projection methods for stochastic dynamic systems: A frequency domain approach

S.E. Pryse[a,*], A. Kundu[b], S. Adhikari[a]

[a] *Zienkiewicz Centre for Computational Engineering, College of Engineering, Swansea University, Swansea SA1 8EN, UK*
[b] *School of Engineering, Cardiff University, Cardiff, CF243 AA, UK*

Received 11 December 2017; received in revised form 23 March 2018; accepted 13 April 2018
Available online 1 May 2018

Abstract

A collection of hybrid projection approaches are proposed for approximating the response of stochastic partial differential equations which describe structural dynamic systems. In this study, an optimal basis for the approximation of the response of a stochastically parametrised structural dynamic system has been computed from its generalised eigenmodes. By applying appropriate approximations in conjunction with a reduced set of modal basis functions, a collection of hybrid projection methods are obtained. These methods have been further improved by the implementation of a sample based Galerkin error minimisation approach. In total six methods are presented and compared for numerical accuracy and computational efficiency. Expressions for the lower order statistical moments of the hybrid projection methods have been derived and discussed. The proposed methods have been implemented to solve two numerical examples: the bending of a Euler–Bernoulli cantilever beam and the bending of a Kirchhoff–Love plate where both structures have stochastic elastic parameters. The response and accuracy of the proposed methods are subsequently discussed and compared with the benchmark solution obtained using an expensive Monte Carlo method.

Keywords: Stochastic differential equations; Eigenfunctions; Galerkin; Finite element; Projection methods; Reduced methods

1. Introduction

The analysis of complex stochastically parametrised engineering structures has recently received significant interest. One of the main factors affecting the analysis is the computational cost associated with computing the response of a system. This can be mainly attributed to the dimension of the structure under consideration. In order address this issue, this paper proposes and compares a set of projection methods that approximates the response of dynamic structures with stochastic parameters.

In this work, stochastic linear damped structural dynamic systems are considered. The stochastic parameter associated with our governing hyperbolic partial differential equation can be characterised by a random parameter

* Corresponding author.
E-mail address: 656060@swansea.ac.uk (S.E. Pryse).

https://doi.org/10.1016/j.cma.2018.04.025
0045-7825/

$a(\mathbf{x}, \theta)$ on a bounded domain on $\mathbb{R}^d$ and a probability space $(\Theta, \mathcal{F}, P)$, where $\theta \in \Theta$ is a sample point from the sampling space Θ, $\mathcal{F}$ is the complete σ-algebra over the subsets of Θ and P is the probability measure. The displacement function of the system is given by $\mathbf{u}(\mathbf{x}, t, \theta)$. $\mathbf{x} \in \mathbb{R}^d$ represents a spatial position vector where d is the number of spatial dimensions and $t \in \mathbb{R}^+$ represents the time. Through the use of well established stochastic finite element methods, a set of discretised linear equations can be obtained to represent the partial differential equations. Numerous methods have been suggested in order to solve or approximate the solution of the discretised set of equations.

Direct Monte Carlo simulation has been widely used in collaboration with stochastic finite element methods to generate the system response at an arbitrarily large number of sample points covering the input parameter space, following which the lower order statistical moments of the quantities of interest are calculated [1,2]. However this method is not favoured for the simulation of large systems. This is due to the convergence of the direct Monte Carlo simulation being slow with increasing dimension and associated variance of the input stochastic space. In addition to this, computing the exact solution of a high resolution finite element model at every sample point render the method extremely expensive. Several approaches have been proposed to reduce the computational effort. These include centroidal Voronoi tessellations [3], quasi Monte Carlo [4,5], Latin hypercube sampling [6], multilevel Monte Carlo [7], derivative-driven Monte Carlo estimators [8] and subset simulation [9].

Expansion based methods have been explored for approximating the response of the discretised set of equations. The perturbation method expands the stiffness and mass matrices, the forcing vector, and the response vector associated with the stochastic finite element method in terms of a truncated Taylor expansion [10,11]. However, the magnitude of the coefficient of variation associated with this method must be restricted [1]. If the coefficient of variation is increased, additional error may be induced. It has been shown that by combining a Taylor expansion with component mode synthesis, an efficient and accurate representation of the modes of a dynamic stochastic finite element structure can be obtained [12]. A method which is computationally competitive with respect to the perturbation method has been suggested by [13]. The proposed Approximate Principal Deformation Mode (APDM) approach utilises the fact that a systems' stiffness matrix can be expressed as a linear function of the uncertain parameters. Consequently, the APDM method can produce more accurate results for higher values of the coefficient of variation. This method has subsequently been used as a foundation for other uncertainty analysis methods [14,15]. The Neumann expansion method has also been applied to approximate the response vector [16]. This is achieved by expanding the inverse of the random matrix in a binomial type series. Numerous methods have been proposed based upon the Neumann expansion. [17] utilises the Neumann expansion to invert complex valued stiffness matrices whilst [18] proposes an acceleration technique in conjunction with the Neumann expansion. By utilising partial bivariate decomposition and successive matrix inversions [19], Ref. [20] has proposed a method to improve the computational efficiency of the Neumann expansion method.

Another class of methods for solving such problems are projection schemes. By utilising Wiener's 1938 work [21,22] proposed a polynomial chaos expansion (PCE) for stochastic finite elements. This method produces a linear combination of Hermite polynomials and undetermined deterministic coefficients. A generalised form for the PCE was subsequently published by utilising functions from the Askey family of polynomials [23,24]. The PCE approach has been widely used in numerous fields including structural dynamics [25], heat transfer [26] and fluid dynamics [27]. Due to the large computational cost associated with the PCE, numerous cost saving approaches have been suggested [28,29]. Sparse polynomial chaos expansions have been wildly used as a surrogate for full models [30,31]. A stepwise regression method has recently been suggested to build a spare polynomial chaos [32]. The PCE approach has influenced many other recent works. Ref. [33] has analysed the compressive sampling of polynomial chaos expansions, whilst a random discrete L^2 projection on polynomial spaces has also been proposed [34].

Model order reduction techniques, which include proper orthogonal decomposition [35,36], balanced model reduction [37] and reduced basis [38,39] have received attention in recent years. Comprehensive reviews of these techniques have been conducted in [40,41]. Refs. [42,43] have suggested adaptive reduced basis strategies in order to ensure a prescribed level of accuracy for a given output. These adaptive reduced basis methods have embedded a goal-oriented error assessment within their proposed methods. Techniques based upon stochastic response surfaces, where the quantities of interest are computed for certain $\theta \in \Theta$, have also received significant interest in recent years [44–46]. We refer the reader to [47–49] for a more comprehensive review of the field and the literature.

The random eigenfunction expansion method has been utilised in [17] to formulate a reduced random basis. In turn, Galerkin methods have been used in conjunction with eigenfunction projections to analyse the response of structures

which are subjected to both a static load [50] and a dynamic load [51]. However questions still exist regarding the exact nature of these projections. As a result, this study proposes a set of novel hybrid forward uncertainty propagation methods to perform a harmonic analysis of structural systems. Novel improved hybrid solution techniques have been proposed as an extension to the projection methods. These approaches have been incorporated by applying a multiplicative sample based Galerkin method. This addition aims to lower the induced error. All the proposed methods have been applied to two example problems (i) the bending of a cantilever beam (ii) the bending of a Kirchhoff–Love plate. Both structures have been discretised and include random parameters. The proposed methods are subsequently discussed and compared through the use of lower order statistical moments and appropriate relative error estimates. Through the use of the relative error estimates, the open questions that surround the hybrid uncertainty propagation methods can be addressed by identifying an optimal reduced projection.

A short overview of the stochastic finite element method is given in Section 2 and three projection methods are presented in Section 3. Methods for reducing the computational effort associated with the proposed methods are discussed in the proceeding sections. Section 4 discusses a method for approximating the random eigensolutions associated with the methods, whilst Section 5 discusses a modal reduction. A sample based Galerkin error minimising technique is presented in Section 6 for each of the proposed methods. Expressions for the response moments of the different projection methods are discussed in Section 7. Section 8 provides a summary of the proposed methods. The approaches are then compared by applying the methods to a one dimensional stochastic Euler–Bernoulli cantilever beam and to a stochastic Kirchhoff–Love plate in Section 9. A summary of the results and the major findings are presented in Section 10.

2. The stochastic finite element method

2.1. Discretisation of the random field

In order to proceed with the stochastic finite element method, it is necessary to discretise the random field that is associated with the governing equation. We consider the stochastic parameter $a(\mathbf{x}, \theta)$ to be a Gaussian random field with a covariance function $C_a : \mathcal{D} \times \mathcal{D} \to \mathbb{R}$ defined on the domain $\mathcal{D}$. The covariance function is positive definite, symmetric and square bounded. The random field $a(\mathbf{x}, \theta)$ can be expressed by a truncated Karhunen–Loève series expansion. This expansion is achieved by performing a spectral decomposition of the covariance function of the field

$$a(\mathbf{x}, \theta) = a_0(\mathbf{x}) + \sum_{i=1}^{M} \sqrt{\widetilde{\lambda}_i}\,\widetilde{\xi}_i(\theta)\widetilde{\boldsymbol{\phi}}_i(\mathbf{x}) \tag{1}$$

where $a_0(\mathbf{x})$ corresponds to the mean function of the random field and $\widetilde{\xi}_i$ are uncorrelated standard random variables. As the random field under consideration is Gaussian, the random variables are deemed as uncorrelated standard normal random variables with zero mean and a unit variance. $\widetilde{\lambda}_i$ and $\widetilde{\boldsymbol{\phi}}_i(\mathbf{x})$ correspond to the eigenvalues and eigenvectors satisfying the following Fredholm integral equation of the second kind

$$\int_D C_a(\mathbf{x}_1, \mathbf{x}_2)\widetilde{\boldsymbol{\phi}}_j(\mathbf{x}_1)\, d\mathbf{x}_1 = \widetilde{\lambda}_j\widetilde{\boldsymbol{\phi}}_j(\mathbf{x}_2) \qquad \forall\ j = 1, 2, \ldots. \tag{2}$$

If the eigenvalues rapidly decay, the value of M could be kept relatively small in order to obtain an accurate depiction of the Gaussian random field. However as the correlation length of the process tends to zero, the number of terms required to obtain an accurate representation would increase.

2.2. Formulating dynamic systems in the frequency domain through finite element modelling

The methods of obtaining the discretised random form of the governing partial differential equations are well-established in stochastic finite element literature. By utilising the finite element method the equations of motion for a multiple-degrees-of-freedom structural vibration problem can be expressed as

$$\mathbf{M}(\theta)\ddot{\mathbf{u}}(t) + \mathbf{C}_0\dot{\mathbf{u}}(t) + \mathbf{K}(\theta)\mathbf{u}(t) = \mathbf{f}_0(t) \tag{3}$$

with the initial conditions set as

$$\mathbf{u}(0) = 0 \in \mathbb{R}^N \qquad \text{and} \qquad \dot{\mathbf{u}}(0) = 0 \in \mathbb{R}^N. \tag{4}$$

In Eq. (3) $\mathbf{M}(\theta)$ and $\mathbf{K}(\theta)$ denote the random mass and stiffness matrices respectively. $\mathbf{C}_0$ and $\mathbf{f}_0(t)$ denote the deterministic damping matrix and the deterministic applied force whilst t represents the time. The displacement is represented by $\mathbf{u}(t)$ and the first and second derivatives of the displacement with respect to time are represented by $\dot{\mathbf{u}}(t)$ and $\ddot{\mathbf{u}}(t)$ respectively. The random mass and stiffness matrices can be expressed as follows

$$\mathbf{M}(\theta) = \mathbf{M}_0 + \sum_{j=1}^{p_1} \mu_j(\theta)\mathbf{M}_j \tag{5}$$

$$\mathbf{K}(\theta) = \mathbf{K}_0 + \sum_{j=1}^{p_2} \nu_j(\theta)\mathbf{K}_j. \tag{6}$$

In the above expressions, $\mathbf{M}_0$ corresponds to the deterministic mass matrix and $\mathbf{K}_0$ to the deterministic stiffness matrix. $\mathbf{M}_i$ and $\mathbf{K}_i$ are symmetric matrices which contribute towards the random components of $\mathbf{M}(\theta)$ and $\mathbf{K}(\theta)$. The random mass matrix has been modelled with p_1 random variables whilst the random stiffness matrix contains p_2 random variables. $\mu_i(\theta)$ represents the random variables associated with the random mass matrix, and $\nu_i(\theta)$ represents the random variables associated with the random stiffness matrix. $\boldsymbol{\zeta}$ denotes a diagonal matrix which contains modal damping factors, thus

$$\boldsymbol{\zeta} = \text{diag}[\zeta_1, \zeta_2, \dots \zeta_N] \in \mathbb{R}^{N\times N}. \tag{7}$$

It is assumed that the all the diagonal entries are equal, therefore $\zeta_1 = \zeta_2 = \cdots = \zeta_N$. In order to satisfy this condition, the damping matrix $\mathbf{C}_0$ takes the following form [52]

$$\mathbf{C}_0 = 2\boldsymbol{\zeta}\mathbf{M}_0\sqrt{\mathbf{M}_0^{-1}\mathbf{K}_0}. \tag{8}$$

We have made the assumption that the deterministic damping matrix belongs to the class of proportional damping matrices [52]. Therefore, the deterministic damping matrix has been simultaneously diagonalised with the mass and stiffness matrices by utilising the deterministic undamped eigenmodes. The detailed discussion of general non-proportional damping is beyond the scope of the present paper. In order to compute the dynamic response in the frequency domain, the Laplace transform of Eq. (3) is considered. Taking the Fourier transform of Eq. (3) results in

$$[-\omega^2\mathbf{M}(\theta) + \mathrm{i}\omega\mathbf{C}_0 + \mathbf{K}(\theta)]\tilde{\mathbf{u}}(\omega, \theta) = \tilde{\mathbf{f}}_0(\omega). \tag{9}$$

Here $\tilde{\mathbf{u}}$ and $\tilde{\mathbf{f}}_0$ are the dynamic response and the forcing in the frequency domain. The random variables associated with both the random mass and the stiffness matrices can be grouped so that $\xi_j(\theta) = \mu_j(\theta)$ for $j = 1, 2, \dots p_1$ and $\xi_{j+p_1}(\theta) = \nu_j(\theta)$ for $j = 1, 2, \dots p_2$. In turn, Eq. (9) can be re-written and expressed as

$$\left(\mathbf{D}_0(\omega) + \sum_{j=1}^{M} \xi_j(\theta)\mathbf{D}_j(\omega)\right)\tilde{\mathbf{u}}(\omega, \theta) = \tilde{\mathbf{f}}_0(\omega) \tag{10}$$

where $\mathbf{D}_0(\omega) \in \mathbb{C}^{N\times N}$ represents the complex deterministic part of the system and $\mathbf{D}_j(\omega) \in \mathbb{R}^{N\times N}$ the random components. The total number of random variables, M, can be computed through summing p_1 and p_2. For the given configuration, the expressions for $\mathbf{D}_0$ and $\mathbf{D}_j$ are as follows

$$\mathbf{D}_0(\omega) = -\omega^2\mathbf{M}_0 + \mathrm{i}\omega\mathbf{C}_0 + \mathbf{K}_0 \tag{11}$$

$$\begin{aligned} \mathbf{D}_j(\omega) &= -\omega^2\mathbf{M}_j \qquad \text{for} \quad j = 1, 2, \dots, p_1 \\ \mathbf{D}_j(\omega) &= \mathbf{K}_{j-p_1} \qquad \text{for} \quad j = p_1 + 1, p_1 + 2, \dots, p_1 + p_2. \end{aligned} \tag{12}$$

Therefore by combining the definitions of $\mathbf{D}_0(\omega)$ and $\mathbf{D}_j(\omega)$ with Eq. (10), all the necessary components have been obtained in order to solve the discretised system of equations in the frequency domain. In the subsequent sections, different projection methods for efficiently approximating the response are compared. This is done for $\theta \in \boldsymbol{\Theta}$ and for every frequency value $\omega \in \Omega$. We refer the reader to [53] for a discussion regarding certain issues that incur during the application of the stochastic finite element method.

3. Derivation of the projection methods

We will initially consider three different projection methods. In order to compare the accuracy and effectiveness of the three proposed methods, a benchmark solution can be obtained by implementing a direct Monte Carlo approach $[DMCS]$

$$\tilde{\mathbf{u}}_{DMCS}(\omega,\theta) = [-\omega^2\mathbf{M}(\theta) + \mathrm{i}\omega\mathbf{C}_0 + \mathbf{K}(\theta)]^{-1}\tilde{\mathbf{f}}_0(\omega) \tag{13}$$

for each frequency and realisation.

We aim to propose a set of methods which computes the response vector by projecting onto a basis with scalar coefficients. The rationale behind proposing different methods is to analyse the effect of the nature of the coefficients and their associated vectors. The first three methods under consideration have the following characteristics:

- Projecting onto a stochastic basis with stochastic coefficients.
- Projecting onto a deterministic basis with stochastic coefficients.
- Projecting onto a deterministic basis with deterministic coefficients.

For all methods, we aim to keep the basis vector independent of the frequency. This is done in an attempt to reduce the computational effort if more than one frequency value were to be analysed. We initially consider the case which incorporates the whole stochastic nature of Eq. (10). For this method, we aim to represent the response by projecting onto a stochastic basis with stochastic coefficients

$$\tilde{\mathbf{u}}_1(\omega,\theta) = \sum_{j=1}^{N} \alpha_j(\omega,\theta)\mathbf{a}_j(\theta) \tag{14}$$

where $\alpha_j(\omega,\theta) \in \mathbb{C}$ denotes the random scalars which are contained in $\boldsymbol{\alpha}(\omega,\theta) \in \mathbb{C}^N$, and $\mathbf{a}_j(\theta) \in \mathbb{C}^N$ denotes the stochastic basis. These basis are contained within the matrix $\mathbf{a}(\theta) \in \mathbb{C}^{N\times N}$. The values of $\alpha_j(\omega,\theta)$ and $\mathbf{a}_j(\theta)$ can be obtained through numerous approaches. One such approach is by solving the following multi-objective optimisation problem

$$\hat{\boldsymbol{\alpha}}(\omega,\theta) = \underset{\boldsymbol{\alpha}\in\mathbb{C}^N}{\arg\min} \ \|\tilde{\mathbf{u}}_{DMCS}(\omega,\theta) - \sum_{j=1}^{N} \alpha_j(\omega,\theta)1\hat{\mathbf{a}}_j(\theta)\|_{L_2(\Theta)\times\mathbb{R}^N} \tag{15}$$

$$\hat{\mathbf{a}}(\theta) = \underset{\mathbf{a}\in\mathbb{C}^{N\times N}}{\arg\min} \ \|\tilde{\mathbf{u}}_{DMCS}(\omega,\theta) - \sum_{j=1}^{N} \hat{\alpha}_j(\theta)\mathbf{a}_j(\omega,\theta)\|_{L_2(\Theta)\times\mathbb{R}^N}. \tag{16}$$

While the above approach gives the generic framework for the evaluation of the $\boldsymbol{\alpha}(\omega,\theta)$ and $\mathbf{a}(\theta)$, the process can be computationally expensive due to the method's slow convergence rate. Furthermore the method could be numerically unstable as the solution may not be unique. In order to avoid calculating $\tilde{\mathbf{u}}_{DMCS}(\omega,\theta)$, an expression for the above L_2 relative error can be obtained by observing the residual and by noting that the approximate error of the solution obtained when using Eq. (14) is

$$\hat{\varepsilon}(\omega,\theta) = \tilde{\mathbf{u}}_1(\omega,\theta) - \tilde{\mathbf{u}}_{DMCS}(\omega,\theta). \tag{17}$$

Here the error measure is defined by using the $DMCS$ approach as a benchmark solution. A closed form of the error in the domain space of $\mathbf{D}(\omega,\theta)$ can be obtained. The residual can be re-written as

$$\mathbf{r}(\omega,\theta) = \mathbf{D}(\omega,\theta)\tilde{\mathbf{u}}_1(\omega,\theta) - \tilde{\mathbf{f}}_0(\omega) = \mathbf{D}(\omega,\theta)\left[\tilde{\mathbf{u}}_1(\omega,\theta) - \tilde{\mathbf{u}}^*(\omega,\theta)\right] \tag{18}$$

where $\tilde{\mathbf{u}}^*(\omega,\theta)$ is the true solution of the system which cannot be evaluated exactly. We can treat the solution of the $DMCS$ approach, $\tilde{\mathbf{u}}_{DMCS}(\omega,\theta)$, as the benchmark solution. It is assumed the $DMCS$ approach gives a better approximation of the true solution compared to $\tilde{\mathbf{u}}_1(\omega,\theta)$. Using $\mathbf{e}(\omega,\theta) = \tilde{\mathbf{u}}_1(\omega,\theta) - \tilde{\mathbf{u}}^*(\omega,\theta)$ as the true error, we write following Eq. (18)

$$\mathbf{D}(\omega,\theta)\mathbf{e}(\omega,\theta) = \mathbf{r}(\omega,\theta). \tag{19}$$

Thus the resulting true error vector is obtained as

$$\mathbf{e}(\omega,\theta) = \mathbf{D}^{-1}(\omega,\theta)\mathbf{r}(\omega,\theta). \tag{20}$$

But $\mathbf{e}(\omega,\theta)$ cannot be computed exactly and we have to resort to the approximate error indicator. We can define a bilinear form as $\bar{\mathbf{D}}(\mathbf{a},\mathbf{b}) = \langle \mathbf{D}(\omega,\theta)\mathbf{a}(\omega,\theta), \mathbf{b}(\omega,\theta)\rangle$ where $\langle\cdot,\cdot\rangle$ denotes an inner product in $L_2(\Theta)\times\mathbb{R}^N$. Hence, from Eq. (20) we can deduce

$$\bar{\mathbf{D}}(\mathbf{e},\hat{\varepsilon}) = R_{\hat{\varepsilon}} \quad \text{where} \quad R_{\hat{\varepsilon}} = \left\langle \mathbf{r}(\omega,\theta), \hat{\varepsilon}(\omega,\theta)\right\rangle. \tag{21}$$

Using Cauchy–Schwarz inequality, we have

$$\left|\bar{\mathbf{D}}(\mathbf{e},\hat{\varepsilon})\right|^2 \le \bar{\mathbf{D}}(\mathbf{e},\mathbf{e})\,\bar{\mathbf{D}}(\hat{\varepsilon},\hat{\varepsilon}) = \|\mathbf{e}\|_E\,\|\hat{\varepsilon}\|_E \tag{22}$$

where $\|\cdot\|_E$ denotes the norm consistent with the bilinear form $\bar{\mathbf{D}}(\cdot,\cdot)$ on $L_2(\Theta)\times\mathbb{R}^N$ (analogous to the elastic potential energy norm for structural dynamic systems). Combining Eqs. (21) and (22) we obtain

$$\frac{|R_{\hat{\varepsilon}}|^2}{\|\hat{\varepsilon}\|_E} \le \|\mathbf{e}\|_E \tag{23}$$

which indicates a lower bound for the true error $\mathbf{e}(\omega,\theta)$ in terms of the approximate error indicator $\hat{\varepsilon}(\omega,\theta)$. The equality holds only under special circumstances which have been detailed in [54]. However as the computation capacity required to implement such an approach is vastly higher than that required for the benchmark solution, a different approach is needed.

3.1. Projecting onto a stochastic basis with stochastic coefficients (*M*1)

In order to implement a different approach, the generalised eigenvalue problem for the undamped case is initially considered

$$\mathbf{K}(\theta)\boldsymbol{\phi}_k(\theta) = \lambda_k(\theta)\mathbf{M}(\theta)\boldsymbol{\phi}_k(\theta); \quad k = 1,2,\ldots,N \tag{24}$$

where $\lambda_k(\theta)$ and $\boldsymbol{\phi}_k(\theta)$ are the kth undamped random eigenvalue and eigenvector. For convenience, matrices that contain the whole set of random eigenvalues and eigenvectors are defined as follows

$$\begin{aligned}&\boldsymbol{\Omega}^2(\theta) = \operatorname{diag}\left[\lambda_1(\theta),\lambda_2(\theta),\ldots,\lambda_n(\theta)\right] \in \mathbb{R}^{N\times N} \quad \text{and}\\ &\boldsymbol{\Phi}(\theta) = \left[\boldsymbol{\phi}_1(\theta),\boldsymbol{\phi}_2(\theta),\ldots,\boldsymbol{\phi}_n(\theta)\right] \in \mathbb{R}^{N\times N}.\end{aligned} \tag{25}$$

The eigenvalues are arranged in ascending order so $\lambda_1(\theta) < \lambda_2(\theta) < \cdots < \lambda_n(\theta)$ and their corresponding eigenvectors are mass normalised and arranged in the same order. It is apparent that

$$\begin{aligned}&\boldsymbol{\Phi}^T(\theta)\mathbf{M}(\theta)\boldsymbol{\Phi}(\theta) = \mathbf{I}\\ &\boldsymbol{\Phi}^T(\theta)\mathbf{K}(\theta)\boldsymbol{\Phi}(\theta) = \boldsymbol{\Omega}^2(\theta).\end{aligned} \tag{26}$$

As the undamped eigenvectors from a complete basis, it is possible to obtain the response of Eq. (10) through projecting on the undamped eigenvectors. This can be done through using the above identities. The Laplace transform of Eq. (3) is initially reconsidered

$$[-\omega^2\mathbf{M}(\theta) + \mathrm{i}\omega\mathbf{C}_0 + \mathbf{K}(\theta)]\tilde{\mathbf{u}}(\omega,\theta) = \tilde{\mathbf{f}}_0(\omega). \tag{27}$$

The modal damping matrix is defined as follows

$$\mathbf{C}'(\theta) = \boldsymbol{\Phi}^T(\theta)\mathbf{C}_0\boldsymbol{\Phi}(\theta) = 2\boldsymbol{\zeta}\boldsymbol{\Omega}(\theta) \tag{28}$$

where $\boldsymbol{\zeta}$ corresponds to the diagonal modal damping matrix introduced in Eq. (7). By using the following modal transformation $\tilde{\mathbf{u}}(\omega,\theta) = \boldsymbol{\Phi}(\theta)\bar{\mathbf{y}}(\omega,\theta)$ and by pre-multiplying Eq. (27) with $\boldsymbol{\Phi}^T(\theta)$, we obtain

$$\boldsymbol{\Phi}^T(\theta)\left\{[-\omega^2\mathbf{M}(\theta) + \mathrm{i}\omega\mathbf{C}_0 + \mathbf{K}(\theta)]\boldsymbol{\Phi}(\theta)\right\}\bar{\mathbf{y}}(\omega,\theta) = \boldsymbol{\Phi}^T(\theta)\tilde{\mathbf{f}}_0(\omega). \tag{29}$$

By combining the modal damping matrix and the orthogonality relationships defined above, it can be shown that

$$\left[-\omega^2\mathbf{I} + 2\mathrm{i}\omega\boldsymbol{\zeta}\boldsymbol{\Omega}(\theta) + \boldsymbol{\Omega}^2(\theta)\right]\bar{\mathbf{y}}(\omega,\theta) = \boldsymbol{\Phi}^T(\theta)\tilde{\mathbf{f}}_0(\omega). \tag{30}$$

Then by inverting $\left[-\omega^2\mathbf{I} + 2\mathrm{i}\omega\boldsymbol{\zeta}\boldsymbol{\Omega}(\theta) + \boldsymbol{\Omega}^2(\theta)\right]$, one has

$$\bar{\mathbf{y}}(\omega,\theta) = \left[-\omega^2\mathbf{I} + 2\mathrm{i}\omega\boldsymbol{\zeta}\boldsymbol{\Omega}(\theta) + \boldsymbol{\Omega}^2(\theta)\right]^{-1}\boldsymbol{\Phi}^T\tilde{\mathbf{f}}_0(\omega). \tag{31}$$

As $\left[-\omega^2\mathbf{I} + 2\mathrm{i}\omega\boldsymbol{\zeta}\boldsymbol{\Omega}(\theta) + \boldsymbol{\Omega}^2(\theta)\right]$ is a diagonal matrix, its inverse is easy to compute and computationally inexpensive. By pre-multiplying both sides of the above equation with $\boldsymbol{\Phi}(\theta)$, we have

$$\boldsymbol{\Phi}(\theta)\bar{\mathbf{y}}(\omega,\theta) = \boldsymbol{\Phi}(\theta)\left[-\omega^2\mathbf{I} + 2\mathrm{i}\omega\boldsymbol{\zeta}\boldsymbol{\Omega}(\theta) + \boldsymbol{\Omega}^2(\theta)\right]^{-1}\boldsymbol{\Phi}^T(\theta)\tilde{\mathbf{f}}_0(\omega). \tag{32}$$

By reintroducing $\tilde{\mathbf{u}}(\omega,\theta)$ for $\boldsymbol{\Phi}(\theta)\bar{\mathbf{y}}(\omega,\theta)$ a dynamic response in the frequency domain can be obtained

$$\tilde{\mathbf{u}}_1(\omega,\theta) = \boldsymbol{\Phi}(\theta)\left[-\omega^2\mathbf{I} + 2\mathrm{i}\omega\boldsymbol{\zeta}\boldsymbol{\Omega}(\theta) + \boldsymbol{\Omega}^2(\theta)\right]^{-1}\boldsymbol{\Phi}^T(\theta)\tilde{\mathbf{f}}_0(\omega). \tag{33}$$

This expression can then be rewritten as a summation, where N corresponds to the number of degrees of freedom associated with the dynamic structure

$$\tilde{\mathbf{u}}_1(\omega,\theta) = \sum_{j=1}^{N}\alpha_j(\omega,\theta)\mathbf{a}_j(\theta) = \sum_{j=1}^{N}\left(\frac{\boldsymbol{\phi}_j^T(\theta)\tilde{\mathbf{f}}_0(\omega)}{\lambda_j(\theta) - \omega^2 + 2\mathrm{i}\sqrt{\lambda_j(\theta)}\omega\zeta}\right)\boldsymbol{\phi}_j(\theta). \tag{34}$$

The response of the dynamic stochastic system under consideration has been represented in the same form as Eq. (14). The random scalars, $\alpha_j(\omega,\theta)$, correspond to the result of $\frac{\boldsymbol{\phi}_j^T(\theta)\tilde{\mathbf{f}}_0}{\lambda_j(\theta)-\omega^2+2\mathrm{i}\sqrt{\lambda_j(\theta)}\omega\zeta}$. In turn, these random scalars are projected onto the space spanned by $\boldsymbol{\phi}_j(\theta)$.

3.2. Projecting onto a deterministic basis with stochastic coefficients (M2)

Thus far one projection method has been proposed through Eq. (34) where both the basis and the projection coefficients are stochastic in nature. If the value of N is large, the computational effort associated with computing the undamped random eigenvalues and eigenvectors can be considered very high. This is especially true if we sample for every $\theta \in \Theta$. In an attempt to lower the computational effort, we will consider a method that projects random scalars onto a deterministic basis

$$\tilde{\mathbf{u}}_2(\omega,\theta) = \sum_{j=1}^{N}\beta_j(\omega,\theta)\mathbf{b}_j. \tag{35}$$

The polynomial chaos approach is a method which projects onto a deterministic basis with stochastic coefficients

$$\tilde{\mathbf{u}}_2(\omega,\theta) = \sum_{k=1}^{P}H_k(\xi(\theta))\mathbf{u}_k(\omega) \tag{36}$$

where $H_k(\xi(\theta))$ represents the polynomial chaoses (corresponding to the random scalars) and $\mathbf{u}_k$ represents unknown deterministic vectors that need to be determined. The value of P is governed by the value of M and by the order of the polynomial chaos expansion. However the polynomial chaos approach is a notoriously costly method if the value of P or N is high. More importantly the basis $\mathbf{u}_k$ is a function of ω, thus this method does not comply with the desired form stated earlier in this section.

Although mathematically erroneous, this paper proposes a method that combines undamped random eigenvalues with undamped deterministic eigenvectors. By exchanging the undamped random eigenvectors seen in Eq. (34) for their deterministic counterparts, the response vector for this new method can be expressed as

$$\tilde{\mathbf{u}}_2(\omega,\theta) = \sum_{j=1}^{N}\left(\frac{\boldsymbol{\phi}_{0_j}^T\tilde{\mathbf{f}}_0}{\lambda_j(\theta) - \omega^2 + 2\mathrm{i}\sqrt{\lambda_j(\theta)}\omega\zeta}\right)\boldsymbol{\phi}_{0_j} \tag{37}$$

where $\boldsymbol{\phi}_{0_j}$ denotes the jth deterministic undamped eigenvector. Therefore we aim to see if the vast majority of the stochastic nature of the system can be incorporated by only using the undamped random eigenvalues.

3.3. Projecting onto a deterministic basis with deterministic coefficients (M3)

As a worst-case scenario we consider the case of when all the eigensolutions are deemed deterministic. For this case, the response vector takes the following form

$$\tilde{\mathbf{u}}_3(\omega,\theta) = \sum_{j=1}^{N}\gamma_{0_j}(\omega)\mathbf{c}_j \tag{38}$$

where $\gamma_{0_j}(\omega) \in \mathbb{C}$ and $\mathbf{c}_j \in \mathbb{C}^N$ are deterministic scalars and basis respectively. If both the undamped random eigenvalues and eigenvectors seen in Eq. (34) are exchanged for their deterministic counterpart, the response vector can be expressed as

$$\tilde{\mathbf{u}}_3(\omega) = \sum_{j=1}^{N} \left(\frac{\boldsymbol{\phi}_{0_j}^T \tilde{\mathbf{f}}_0}{\lambda_{0_j} - \omega^2 + 2\mathrm{i}\sqrt{\lambda_{0_j}}\omega\zeta} \right) \boldsymbol{\phi}_{0_j} \tag{39}$$

where λ_{0_j} and $\boldsymbol{\phi}_{0_j}$ denote the jth undamped deterministic eigenvalue and eigenvector respectively. Due to all the terms in Eq. (39) being deterministic, the stochastic nature of the system is not at all incorporated into the response vector. It can be deduced that Eq. (39) provides the deterministic solution and therefore can be established as a worst case scenario. However if the coefficient of variation associated with the stochastic process is low, this method could provide an adequate approximation of the mean of the true solution.

If the matrices $\mathbf{U}_{DMCS} \in \mathbb{C}^{N\times m}$ and $\mathbf{U}_3 \in \mathbb{C}^{N\times m}$ contain the solution vectors for all realisations of a given frequency for the benchmark and $M3$ methods, the Frobenius norm of the relative error is given by

$$\|\mathbf{U}_{DMCS} - \mathbf{U}_3\|_F = \sqrt{\sum_{i=1}^{N}\sum_{j=1}^{m} \left|\{\mathbf{U}_{DMCS} - \mathbf{U}_3\}_{ij}\right|^2} \tag{40}$$

where m corresponds to the number of realisations. If the matrices $\mathbf{U}_1 \in \mathbb{C}^{N\times m}$ and $\mathbf{U}_2 \in \mathbb{C}^{N\times m}$ are similarly defined for the $M1$ and $M2$ methods the following propositions can be made

$$\|\mathbf{U}_{DMCS} - \mathbf{U}_1\|_F \leq \|\mathbf{U}_{DMCS} - \mathbf{U}_2\|_F \leq \|\mathbf{U}_{DMCS} - \mathbf{U}_3\|_F. \tag{41}$$

Due to both the eigenvalues and the eigenvectors retaining their stochastic properties in $M1$ method, it is intuitively expected that the $M1$ method would induce the least amount of error. As the entire stochasticity of the response vector is expected to be captured by the stochastic eigenvalues in the $M2$ method, this method is not expected to outperform the $M1$ method. In a similar manner, as the $M3$ is deemed to be a worst-case scenario, naturally this method will not outperform both the $M1$ and $M2$ methods.

At present, the computational time associated with both the $M1$ and $M2$ methods can be considered quite high, especially for a high degree of freedom finite element system. This is due to two reasons. The first being the large number of terms in the summations seen in Eqs. (34) and (37). At present, the number of terms in the series corresponds to the number of degrees of freedom. Secondly, calculating the random eigensolutions is computationally expensive. Combining these reasons with the need to simulate the methods for each $\theta \in \Theta$ accumulates to a high computational effort. These issues have been addressed in the following section where approximation and truncation techniques are introduced.

4. Approximating the undamped eigensolutions

Calculating the exact undamped random eigensolutions can be extremely expensive, especially if the number of degrees of freedom is large. Thus a sensitivity approach to approximate the eigensolutions could computationally be a better option. The set of exact undamped random eigensolutions can be obtained through combining direct Monte Carlo simulations with the eigenvalue problem of the undamped system expressed by Eq. (24). The set of random eigenvalues could consequently be used to obtain the natural frequencies of the system

$$\omega_k(\theta) = \sqrt{\lambda_k(\theta)} \tag{42}$$

where $\omega_k(\theta)$ represents the kth random natural frequency of a realisation. Due to the low computational effort associated with the first order perturbation method, this method has been used to approximate both the undamped random eigenvalues and eigenvectors. The random eigenvalues can be approximated by the following equation

$$\lambda_j \approx \lambda_{j_0} + \sum_{k=1}^{M} \left(\frac{\partial \lambda_j}{\partial \xi_k} \right) \mathrm{d}\xi_k(\theta) \tag{43}$$

where λ_{j_0} is the jth deterministic undamped eigenvalue and $\mathrm{d}\xi_k(\theta)$ a set of Gaussian random variables with mean zero and unit variance. The derivative of the undamped random eigenvalues with respect to ξ_k can be obtained through

differentiating and manipulating the eigenvalue equation denoted by Eq. (24) [55]. This results in the following equation

$$\frac{\partial \lambda_j}{\partial \xi_k} = \frac{\boldsymbol{\phi}_{0_j}^T \left[\frac{\partial \mathbf{K}}{\partial \xi_k} - \lambda_{0_j} \frac{\partial \mathbf{M}}{\partial \xi_k} \right] \boldsymbol{\phi}_{0_j}}{\boldsymbol{\phi}_{0_j}^T \mathbf{M}_0 \boldsymbol{\phi}_{0_j}} \tag{44}$$

where λ_{0_j} and ϕ_{0_j} correspond to the deterministic undamped eigenvalues and eigenvectors. As the deterministic undamped eigenvectors are mass normalised, the denominator in the above equation equates to one i.e. $\boldsymbol{\phi}_{0_j}^T \mathbf{M}_0 \boldsymbol{\phi}_{0_j} = 1$, thus resulting in

$$\frac{\partial \lambda_{0_j}}{\partial \xi_k} = \boldsymbol{\phi}_{0_j}^T \left[\frac{\partial \mathbf{K}}{\partial \xi_k} - \lambda_{0_j} \frac{\partial \mathbf{M}}{\partial \xi_k} \right] \boldsymbol{\phi}_{0_j}. \tag{45}$$

In the instance of Eq. (45), the values of both $\frac{\partial \mathbf{M}}{\partial \xi_k}$ and $\frac{\partial \mathbf{K}}{\partial \xi_k}$ are as follows

$$\begin{aligned} \frac{\partial \mathbf{M}}{\partial \xi_k} &= \begin{cases} \mathbf{M}_k, & \text{for } j = 1, 2, \ldots, p_1 \\ 0, & \text{otherwise} \end{cases} \\ \frac{\partial \mathbf{K}}{\partial \xi_k} &= \begin{cases} \mathbf{K}_{k-p_1}, & \text{for } k = p_1 + 1, p_1 + 2, \ldots, p_1 + p_2 \\ 0, & \text{otherwise} \end{cases} \end{aligned} \tag{46}$$

where $\mathbf{M}_k$ and $\mathbf{K}_k - p_1$ correspond to the random components of $\mathbf{M}(\theta)$ and $\mathbf{K}(\theta)$ introduced through Eqs. (5) and (6).

In a similar manner, the random undamped eigenvectors can also be expressed by a first-order perturbation

$$\boldsymbol{\phi}_j \approx \boldsymbol{\phi}_{j_0} + \sum_{k=1}^{M} \left(\frac{\partial \boldsymbol{\phi}_j}{\partial \xi_k} \right) \mathrm{d}\xi_k(\theta) \tag{47}$$

where $\boldsymbol{\phi}_{j_0}$ is the jth deterministic undamped eigenvector and $\mathrm{d}\xi_k(\theta)$ a set of Gaussian random variables with mean zero and unit variance. It is possible to obtain the derivative of the jth undamped random eigenvector with respect to ξ_k by expressing the result as a linear combination of deterministic eigenvectors. This can be illustrated by

$$\frac{\partial \boldsymbol{\phi}_j}{\partial \xi_k} = \sum_{r=1}^{N} \alpha_{jr} \boldsymbol{\phi}_{0_r}. \tag{48}$$

The full algebraic detail of obtaining the derivative can be found in [55]. The final expression for $\frac{\partial \boldsymbol{\phi}_j}{\partial \xi_k}$ is given by

$$\frac{\partial \boldsymbol{\phi}_j}{\partial \xi_k} = -\frac{1}{2} \left(\boldsymbol{\phi}_{j_0}^T \frac{\partial \mathbf{M}}{\partial \xi_k} \boldsymbol{\phi}_{j_0} \right) + \sum_{i=1 \neq j}^{N} \frac{\boldsymbol{\phi}_{k_0}^T \left[\frac{\partial \mathbf{K}}{\partial \xi_k} - \lambda_{j_0} \frac{\partial \mathbf{M}}{\partial \xi_k} \right] \boldsymbol{\phi}_{j_0}}{\lambda_{j_0} - \lambda_{k_0}} \boldsymbol{\phi}_{k_0}. \tag{49}$$

The values of both $\frac{\partial \mathbf{M}}{\partial \xi_k}$ and $\frac{\partial \mathbf{K}}{\partial \xi_k}$ are identical to those given in Eq. (46). This method requires all the deterministic eigenvalues and eigenvectors to be known. Furthermore the eigenvalues are required to be unique. For the case of repeated eigenvalues the proposed methods would still be valid, however a different method would be required to approximate the eigenvectors [56].

Thus by approximating the random eigensolutions it can be categorically concluded that the computational effort associated with each of the proposed methods are as follows

$$\mathcal{C}_{M1} > \mathcal{C}_{M2} > \mathcal{C}_{M3} \tag{50}$$

where $\mathcal{C}$ represents the computational effort. Providing that the proposed methods for approximating the eigensolutions are accurate, by comparing Eqs. (41) and (50) it is apparent that a trade-off between the error and the computational effort is present. $M1$ provides the most accurate representation of the response vector however its computational effort is the highest. $M3$ provides the least accurate response, however this is achieved with a considerably lower computational effort.

5. Modal basis reduction

At present all the methods described in Section 3 require the calculation and summation of N terms. In cooperation with the approximations seen in Section 4, these methods can be deemed rather inexpensive in comparison with the

polynomial chaos approach. The polynomial chaos approach requires a set of NP algebraic equations to be solved where P corresponds to the number of polynomial chaoses. However, we aim to lower the computational effort of our proposed methods even further.

Through revisiting the ordering of the eigenvalues seen in Eq. (25) it can be deduced that

$$\lambda_1 < \lambda_2 < \cdots < \lambda_N \tag{51}$$

where λ_j corresponds to the jth eigenvalue. From the scalar terms $\alpha_j(\omega,\theta)$, $\beta_j(\omega,\theta)$ and $\gamma_{0_j}(\omega)$ seen Eqs. (34), (37) and (39), it can be observed that the eigenvalues appear in the denominator. The scalar α_j is shown for illustration

$$\alpha_j(\omega,\theta) = \frac{\boldsymbol{\phi}_j^T(\theta)\tilde{\mathbf{f}}_0}{\lambda_j(\theta) - \omega^2 + 2\mathrm{i}\sqrt{\lambda_j(\theta)}\omega\zeta}. \tag{52}$$

For the values of j satisfying $\lambda_j(\theta) + 2\mathrm{i}\sqrt{\lambda_j(\theta)}\omega\zeta > \omega^2$, it is apparent that the value of the denominator increases as the value of j increases. The value of the numerator depends on the deterministic force $\tilde{\mathbf{f}}_0$ and the undamped eigenvectors. The numerator cannot be ordered in terms of magnitude for different values of j, however due to the mass normalisation of the undamped eigenvectors, it can be deduced that the value of the numerator does not vary significantly. Therefore it is established that the value of $\alpha_j(\omega,\theta)$ generally decreases as the value of j increases. Consequently the upper limits of the summations seen in Eqs. (34), (37) and (39) can be lowered. In turn, these equations can be expressed as

$$\tilde{\mathbf{u}}_1(\omega,\theta) \approx \sum_{j=1}^{n_r} \left(\frac{\boldsymbol{\phi}_j^T(\theta)\tilde{\mathbf{f}}_0}{\lambda_j(\theta) - \omega^2 + 2\mathrm{i}\sqrt{\lambda_j(\theta)}\omega\zeta} \right) \boldsymbol{\phi}_j(\theta) \tag{53}$$

$$\tilde{\mathbf{u}}_2(\omega,\theta) \approx \sum_{j=1}^{n_r} \left(\frac{\boldsymbol{\phi}_{0_j}^T\tilde{\mathbf{f}}_0}{\lambda_j(\theta) - \omega^2 + 2\mathrm{i}\sqrt{\lambda_j(\theta)}\omega\zeta} \right) \boldsymbol{\phi}_{0_j} \tag{54}$$

$$\tilde{\mathbf{u}}_3(\omega) \approx \sum_{j=1}^{n_r} \left(\frac{\boldsymbol{\phi}_{0_j}^T\tilde{\mathbf{f}}_0}{\lambda_{0_j} - \omega^2 + 2\mathrm{i}\sqrt{\lambda_{0_j}}\omega\zeta} \right) \boldsymbol{\phi}_{0_j} \tag{55}$$

respectively, where $n_r < N \ll NP$. The value of n_r can be defined in two ways (a) the value can be predefined depending on the system under consideration (b) by selecting a value for ϵ which is sufficiently small, n_r can be selected such that $\lambda_{0_{(n_r)}}$ is the largest deterministic eigenvalue that satisfies $\frac{\lambda_{0_1}}{\lambda_{0_{(n_r)}}} > \epsilon$. If the accuracy of the truncated series is not sufficient, the accuracy can be improved by increasing the predefined value of n_r or selecting a lower value for ϵ.

6. Sample based Galerkin error minimisation

Three different projection methods have been proposed in Section 3. The first projects random scalars onto a stochastic basis whilst the second projects random scalars onto a deterministic basis. The third method projects deterministic scalars onto a deterministic basis. We have shown that it is possible to approximate the random eigensolutions that arise in the proposed methods in order to lower the computational effort. However these approximations, in addition to the modal reduction introduced in Section 5 introduces error into the calculation. This has motivated an error minimisation technique through applying a sample based Galerkin approach. As a result, in addition to the three projection methods introduced in Section 3, the following three projection methods are proposed:

- Galerkin approach with projecting onto a stochastic basis with stochastic coefficients ($M1G$).
- Galerkin approach with projecting onto a stochastic basis with deterministic coefficients ($M2G$).
- Galerkin approach with projecting onto a deterministic basis with deterministic coefficients ($M3G$).

The case of incorporating a sample based Galerkin approach with projecting onto a stochastic basis with stochastic coefficients is initially considered.

6.1. Galerkin approach with projecting onto a stochastic basis with stochastic coefficients (M1G)

The response vector for the given case is modified to take the following series representation

$$\begin{aligned}\tilde{\mathbf{u}}_{1G}(\omega,\theta) &\approx \sum_{j=1}^{n_r} c_j(\omega,\theta)\left(\frac{\boldsymbol{\phi}_j^T(\theta)\tilde{\mathbf{f}}_0}{\lambda_j(\theta)-\omega^2+2\mathrm{i}\sqrt{\lambda_j(\theta)}\omega\zeta}\right)\boldsymbol{\phi}_j(\theta)\\ &= \sum_{j=1}^{n_r} c_j\left(\omega,\theta\right)\alpha_j\left(\omega,\theta\right)\boldsymbol{\phi}_j\left(\theta\right).\end{aligned} \tag{56}$$

Here $\alpha_j(\omega,\theta)$ and $\boldsymbol{\phi}_j(\theta)$ correspond to the random scalars and random eigenvectors seen in Eq. (34) whilst $c_j\left(\omega,\theta\right) \in \mathbb{C}$ are constants which need to be obtained for each realisation. This can be done by applying a sample based Galerkin approach. We initially consider the following residual

$$\mathbf{r}(\omega,\theta) = \left(\sum_{i=0}^{M}\mathbf{D}_i(\omega)\xi_i(\theta)\right)\left(\sum_{j=1}^{n_r} c_j(\omega,\theta)\alpha_j(\omega,\theta)\boldsymbol{\phi}_j(\theta)\right) - \tilde{\mathbf{f}}_0(\omega) \in \mathbb{C}^N \tag{57}$$

where $\xi_0 = 1$ is used in order to simplify the summation. $\mathbf{D}_i(\omega)$, $\xi_i(\theta)$ and $\tilde{\mathbf{f}}_0(\omega)$ correspond to the terms arising in Eqs. (9) and (10). By making the residual orthogonal to a basis function, the unknown $c_j(\omega,\theta)$ can be computed. As Eq. (56) can be viewed as a projection onto a stochastic basis, the residual is made orthogonal to the undamped random eigenvectors

$$\mathbf{r}(\omega,\theta) \perp \boldsymbol{\phi}_k(\theta) \qquad \forall \quad k = 1,2,\ldots n_r. \tag{58}$$

As a sample based Galerkin approach is considered, applying the orthogonality condition results in

$$\boldsymbol{\phi}_k^T(\theta)\left[\left(\sum_{i=0}^{M}\mathbf{D}_i(\omega)\xi_i(\theta)\right)\left(\sum_{j=1}^{n_r} c_j(\omega,\theta)\alpha_j(\omega,\theta)\boldsymbol{\phi}_j(\theta)\right) - \boldsymbol{\phi}_k^T(\theta)\tilde{\mathbf{f}}_0(\omega)\right] = 0. \tag{59}$$

Through manipulating Eq. (59) it is possible to re-write the equation in the following form

$$\sum_{j=1}^{n_r}\underbrace{\left(\sum_{i=0}^{M}\left[\boldsymbol{\phi}_k^T(\theta)\mathbf{D}_i(\omega)\boldsymbol{\phi}_j(\theta)\right]\left[\xi_i(\theta)\alpha_j(\omega,\theta)\right]\right)}_{\mathbf{Z}_1(\omega,\theta)}\underbrace{c_j(\omega,\theta)}_{\mathbf{c}_1(\omega,\theta)} = \underbrace{\boldsymbol{\phi}_k^T(\theta)\tilde{\mathbf{f}}_0(\omega)}_{\mathbf{y}_1(\omega)}. \tag{60}$$

By defining the vector $\mathbf{c}_1\left(\omega,\theta\right) = \left[c_1\left(\omega,\theta\right)c_2\left(\omega,\theta\right)\ldots c_{n_r}\left(\omega,\theta\right)\right]^T$, Eq. (60) can be re-written as

$$\mathbf{Z}_1(\omega,\theta)\mathbf{c}_1(\omega,\theta) = \mathbf{y}_1(\omega,\theta) \qquad j,k = 1,2,\ldots,n_r \tag{61}$$

where $\mathbf{Z}_{1_{kj}}(\omega,\theta) = \sum_{i=0}^{M}\left[\boldsymbol{\phi}_k^T(\theta)\mathbf{D}_i(\omega)\boldsymbol{\phi}_j(\theta)\right]\left[\xi_i(\theta)\alpha_j(\omega,\theta)\right]$; $\forall j,k = 1,2,\ldots n_r$ and $\mathbf{y}_1(\omega,\theta) = \boldsymbol{\phi}_k^T(\theta)\tilde{\mathbf{f}}_0(\omega)$. The number of equations that need to be solved in order to calculate the unknown vector $\mathbf{c}(\omega,\theta)$ corresponds to the value of n_r. By increasing the number of terms from n_r to n_r+1, the number of terms in $\mathbf{Z}_1(\omega,\theta)$ increases by $2n+1$. Therefore the lower the dimension of the reduced system, the fewer the number of equations that need to be solved. This is of importance as the given procedure needs to be repeated for every realisation and for every frequency under consideration.

6.2. Galerkin approach with projecting onto a stochastic basis with deterministic coefficients (M2G)

A similar approach can be implemented for the case containing undamped random eigenvalues and deterministic eigenvectors. The response vector for this given approach takes the following form

$$\begin{aligned}\tilde{\mathbf{u}}_{2G}(\omega,\theta) &\approx \sum_{j=1}^{n_r} c_j(\omega,\theta)\left(\frac{\boldsymbol{\phi}_{0_j}^T\tilde{\mathbf{f}}_0}{\lambda_j(\theta)-\omega^2+2\mathrm{i}\sqrt{\lambda_j(\theta)}\omega\zeta}\right)\boldsymbol{\phi}_{0_j}\\ &= \sum_{j=1}^{n_r} c_j\left(\omega,\theta\right)\beta_j\left(\omega,\theta\right)\boldsymbol{\phi}_{0_j}.\end{aligned} \tag{62}$$

Here $\beta_j(\omega,\theta)$ corresponds to the scalars introduced in Eq. (37) and $\boldsymbol{\phi}_{0_j}$ to the deterministic eigenvectors also introduced in Eq. (37). $c_j(\omega,\theta) \in \mathbb{C}$ are the unknown constants that need to obtained for each realisation of each frequency. A similar sample based Galerkin method can be implemented to compute the unknown constants. In order to mimic the projection seen in Eq. (37), the residual is projected onto deterministic eigenvectors rather than the random eigenvectors seen in Section 6.1. By following a similar approach to that seen in Section 6.1, the unknown constants $c_j(\omega,\theta)$ can be computed by solving the following set of linear equations.

$$\mathbf{Z}_2(\omega,\theta)\mathbf{c}_2(\omega,\theta) = \mathbf{y}_2(\omega) \qquad j,k = 1,2,\ldots,n_r \tag{63}$$

where

$$\mathbf{Z}_{2_{kj}}(\omega,\theta) = \sum_{i=0}^{M}\left[\boldsymbol{\phi}_{0_k}^T\mathbf{D}_i(\omega)\boldsymbol{\phi}_{0_j}\right]\left[\xi_i(\theta)\beta_j(\omega,\theta)\right];$$

$$\beta_j(\omega,\theta) = \sum_{j=1}^{n_r}\left(\frac{\boldsymbol{\phi}_{0_j}^T\tilde{\mathbf{f}}_0}{\lambda_j(\theta)-\omega^2+2\mathrm{i}\sqrt{\lambda_j(\theta)}\omega\zeta}\right)$$

$$\mathbf{y}_2(\omega) = \boldsymbol{\phi}_k^T(\theta)\tilde{\mathbf{f}}_0(\omega) \quad \forall \quad j,k = 1,2,\ldots n_r$$

and $\mathbf{c}_2(\omega,\theta)$ is a vector that contains the unknown constants $c_j(\omega,\theta)$.

The number of equations that need to be solved to compute the unknown coefficients corresponds to the number of modes retained in the reduced models in Section 5. Similarly to the method described in Section 6.1, this procedure needs to be repeated for every realisation and for every $\omega \in \Omega$.

6.3. Galerkin approach with projecting onto a deterministic basis with deterministic coefficients (M3G)

A Galerkin approach can also be considered for the case that contains undamped deterministic eigenvalues and eigenvectors. For this case, the response vector is defined as follows

$$\begin{aligned}\tilde{\mathbf{u}}_{3G}(\omega,\theta) &\approx \sum_{j=1}^{n_r} c_j(\omega,\theta)\left(\frac{\boldsymbol{\phi}_{0_j}^T\tilde{\mathbf{f}}_0}{\lambda_{0_j}-\omega^2+2\mathrm{i}\sqrt{\lambda_{0_j}}\omega\zeta}\right)\boldsymbol{\phi}_{0_j}\\ &= \sum_{j=1}^{n_r} c_j(\omega,\theta)\,\gamma_{0_j}(\omega)\,\boldsymbol{\phi}_{0_j}\end{aligned} \tag{64}$$

where $\gamma_{0_j}(\omega)$ and $\boldsymbol{\phi}_{0_j}$ correspond to the deterministic scalars and the undamped deterministic eigenvector introduced in Eq. (39). $c_j(\omega,\theta) \in \mathbb{C}$ are unknown constants which need to obtained for each realisation of each frequency. Similarly to the two preceding methods, by applying a sample based Galerkin approach the unknown constants can be computed. Sequentially, the following set of equations is required to be solved for every realisation in each considered frequency

$$\mathbf{Z}_3(\omega,\theta)\mathbf{c}_3(\omega,\theta) = \mathbf{y}_3(\omega,\theta) \qquad j,k = 1,2,\ldots,n_r \tag{65}$$

where

$$\mathbf{Z}_{3_{kj}}(\omega,\theta) = \sum_{i=0}^{M}\left[\boldsymbol{\phi}_{0_k}^T\mathbf{D}_i(\omega)\boldsymbol{\phi}_{0_j}\right]\left[\xi_i(\theta)\gamma_{0_j}(\omega)\right];$$

$$\gamma_{0_j}(\omega) = \sum_{j=1}^{n_r}\left(\frac{\boldsymbol{\phi}_{0_j}^T\tilde{\mathbf{f}}_0}{\lambda_{0_j}-\omega^2+2\mathrm{i}\sqrt{\lambda_{0_j}}\omega\zeta}\right)$$

$$\mathbf{y}_3(\omega) = \boldsymbol{\phi}_{0_k}^T\tilde{\mathbf{f}}_0(\omega) \quad \forall \quad j,k = 1,2,\ldots n_r$$

and $\mathbf{c}_3(\omega,\theta)$ is the vector that contains the unknown constants $c_j(\omega,\theta)$.

The computational effort associated with this method is considerably lower than the other Galerkin methods as the scalars γ_{0_j} only need to be calculated once for each given frequency. The aim of this method is to incorporate the whole stochastic nature of system within the unknown scalars $c_j(\omega,\theta)$. However it is not known if the Galerkin approach can substantially lower the error as all the eigensolutions used are deterministic. This method is of significant interest as it is known that the behaviour of deterministic and stochastic systems can differ substantially especially if the coefficient of variation is significantly large.

7. Calculation of the response statistics

Calculating response statistics such as the mean and covariance matrices can be deemed fundamental during analysing practical examples. The response statistics given in this section can be computed through implementing the methods described in the previous sections.

The response vector $\tilde{\mathbf{u}}(\omega, \theta)$ is a complex valued random process. The complete statistical characterisation of the response is not only computationally expensive but also difficult to interpellate physically. For this reason we are only interested in the modulus of this quantity. From an engineering point of view, this quantity is of significant interest.

The mean of the modulus of the response vector for a given frequency is defined as

$$\bar{\mathbf{u}}(\omega) = \mathbb{E}\left[\left|\tilde{\mathbf{u}}(\omega, \theta)\right|\right]. \tag{66}$$

Similarly the covariance matrix of a given frequency can be defined as follows

$$\mathbf{C}_{\tilde{\mathbf{u}}}(\omega) = \mathbb{E}\left[\left(|\tilde{\mathbf{u}}(\omega, \theta)| - \mathbb{E}\left[\left|\tilde{\mathbf{u}}(\omega, \theta)\right|\right]\right)\left(|\tilde{\mathbf{u}}(\omega, \theta)| - \mathbb{E}\left[\left|\tilde{\mathbf{u}}(\omega, \theta)\right|\right]\right)^T\right] \in \mathbb{R}^{N\times N} \tag{67}$$

where $\bar{\mathbf{u}}$ corresponds to the mean of the response vector and $(\star)^T$ denotes the transpose of $\star$.

7.1. Response statistics for the $M1$ and $M1G$ methods

The case of a stochastic projection incorporated with stochastic eigensolutions and a Galerkin error minimisation approach ($M1G$) is initially considered. For this case, the response vector can take the following form

$$\tilde{\mathbf{u}}_{1G}(\omega, \theta) = \sum_{j=1}^{n_r} c_j(\omega, \theta)\alpha_j(\omega, \theta)\boldsymbol{\phi}_j(\theta) \tag{68}$$

where $\alpha_j(\omega, \theta)$ corresponds to the random scalars seen in Eq. (56). Defining $\tilde{\mathbf{u}}_{1G}(\omega, \theta)$ in such a way supports neatness whilst calculating response statistics. When analysing the displacement of structures, the modulus of the response corresponds to the maximum displacement or the amplitude seen at each node. The mean vector of the amplitude can be expressed as

$$\bar{\mathbf{u}}_{1G}(\omega) = \sum_{j=1}^{n_r} \mathbb{E}\left[\left|c_j(\omega, \theta)\alpha_j(\omega, \theta)\boldsymbol{\phi}_j(\theta)\right|\right] \tag{69}$$

where $|\star|$ denotes the absolute value of $\star$. By using the expression from Eq. (69), it is possible to define the covariance matrix of the amplitude. In the expression below, rather than using the standard sigma notation, the covariance matrix is defined by $\mathbf{C}$ in order to clarify between the covariance matrix and the summations

$$\begin{aligned}\mathbf{C}_{\tilde{\mathbf{u}}_{1G}}(\omega) = \mathbb{E}\Bigg[&\left(\sum_{j=1}^{n_r}\left|c_j(\omega, \theta)\alpha_j(\omega, \theta)\boldsymbol{\phi}_j(\theta)\right| - \sum_{j=1}^{n_r}\mathbb{E}\left[\left|c_j(\omega, \theta)\alpha_j(\omega, \theta)\boldsymbol{\phi}_j(\theta)\right|\right]\right)\\ &\left(\sum_{k=1}^{n_r}\left|c_k(\omega, \theta)\alpha_k(\omega, \theta)\boldsymbol{\phi}_k(\theta)\right| - \sum_{k=1}^{n_r}\mathbb{E}\left[\left|c_k(\omega, \theta)\alpha_k(\omega, \theta)\boldsymbol{\phi}_k(\theta)\right|\right]\right)^T\Bigg].\end{aligned} \tag{70}$$

Due to the stochastic nature of this approach, the expression for the covariance matrix cannot be simplified. The mean and covariance matrix of the $M1$ method takes a similar form to Eqs. (69) and (70). All the terms are retained, however $c_j = 1 \quad \forall \quad j = 1, 2, \ldots n_r$ and $c_k = 1 \quad \forall \quad k = 1, 2, \ldots n_r$.

7.2. Response statistics for the $M2$ and $M2G$ methods

Similarly to the previous case, the method which incorporates the undamped random eigenvalues, undamped deterministic eigenvector and the Galerkin error minimisation approach ($M2G$) is initially considered. We will consider the method's response vector in following form

$$\tilde{\mathbf{u}}_{2G}(\omega, \theta) = \sum_{j=1}^{n_r} c_j\,(\omega, \theta)\,\beta_j\,(\omega, \theta)\,\boldsymbol{\phi}_{0_j} \tag{71}$$

where $\beta_j(\omega,\theta)$ corresponds to the random scalars seen in Eq. (62). Due to the undamped deterministic eigenvectors, the mean vector of the amplitude can be expressed as

$$\bar{\mathbf{u}}_{2G}(\omega) = \sum_{j=1}^{n_r} \mathbb{E}\left[\left|c_j(\omega,\theta)\alpha_j(\omega,\theta)\right|\right]\left|\boldsymbol{\phi}_{j_0}\right|. \tag{72}$$

In a similar manner to the previous case, the covariance matrix of the amplitude can be expressed by

$$\mathbf{C}_{\tilde{\mathbf{u}}_{2G}}(\omega) = \sum_{j=1}^{n_r}\sum_{k=1}^{n_r} \boldsymbol{\Psi}_{2G}(\omega,\theta)\left|\boldsymbol{\phi}_{0_j}\boldsymbol{\phi}_{0_k}^T\right| \tag{73}$$

where the stochastic terms arising in the covariance matrix are given by

$$\begin{aligned}\boldsymbol{\Psi}_{2G}(\omega,\theta) = \mathbb{E}\Bigg[&\Big(\left|\beta_j(\omega,\theta)c_j(\omega,\theta)\right| - \mathbb{E}\left[\left|\beta_j(\omega,\theta)c_j(\omega,\theta)\right|\right]\Big)\\ &\Big(\left|\beta_k(\omega,\theta)c_k(\omega,\theta)\right| - \mathbb{E}\left[\left|\beta_k(\omega,\theta)c_k(\omega,\theta)\right|\right]\Big)\Bigg].\end{aligned} \tag{74}$$

Due to the undamped eigenvectors being deterministic, less computational effort is needed to compute the expected values arising in the above expression in comparison to that given by Eq. (70). The mean and covariance matrix of the $M2$ method takes a similar form to Eqs. (72) and (73). The only difference is that $c_j = 1 \quad \forall \quad j = 1, 2, \ldots n_r$ and $c_k = 1 \quad \forall \quad k = 1, 2, \ldots n_r$.

7.3. Response statistics for the $M3$ and $M3G$ methods

When analysing the corresponding mean and covariance matrix arising from the $M3$ and $M3G$ methods, substantial computational reduction can be seen due to the introduction of additional deterministic terms. The response vector of the $M3G$ method is initially considered in the following form

$$\tilde{\mathbf{u}}_{3G}(\omega,\theta) = \sum_{j=1}^{n_r} c_j(\omega,\theta)\gamma_{0_j}(\omega)\boldsymbol{\phi}_{0_j} \tag{75}$$

where $\gamma_{0_j}(\omega)$ corresponds to the deterministic scalars seen in Eq. (64). The mean vector of the amplitude can be expressed as

$$\bar{\mathbf{u}}_{3G}(\omega) = \sum_{j=1}^{n_r} \mathbb{E}\left[\left|c_j(\omega,\theta)\right|\right]\left|\gamma_{0_j}(\omega)\boldsymbol{\phi}_{0_j}\right| \tag{76}$$

where the only expected value arising is that of the scalars $c_j(\omega,\theta)$. The same is true when considering the covariance matrix of the amplitude

$$\mathbf{C}_{\tilde{\mathbf{u}}_{3G}}(\omega) = \sum_{j=1}^{n_r}\sum_{k=1}^{n_r} \left|\gamma_{0_j}(\omega)\gamma_{0_k}(\omega)\right| \boldsymbol{\Psi}_{3G}(\omega,\theta)\left|\boldsymbol{\phi}_{0_j}\boldsymbol{\phi}_{0_k}^T\right| \tag{77}$$

where in this instance, the elements of the stochastic term $\boldsymbol{\Psi}_{3G}$ only contain the scalar terms $c_j(\omega,\theta)$ and $c_k(\omega,\theta)$.

$$\boldsymbol{\Psi}_{3G}(\omega,\theta) = \mathbb{E}\Bigg[\Big(\left|c_j(\omega,\theta)\right| - \mathbb{E}\left[\left|c_j(\omega,\theta)\right|\right]\Big)\Big(\left|c_k(\omega,\theta)\right| - \mathbb{E}\left[\left|c_k(\omega,\theta)\right|\right]\Big)\Bigg]. \tag{78}$$

As there are no stochastic terms arising in the response when using the $M3$ method, it can be easily deduced that $\bar{\mathbf{u}}_{3G}(\omega) = \tilde{\mathbf{u}}_{3G}(\omega)$. Consequently, the covariance matrix would take the form of the zero matrix.

8. Summary of the proposed methods

Thus far six projection methods have been proposed in order to analyse the response of stochastically parametrised structural dynamic systems. The first three methods analyse the effect of altering the nature of the coefficients and their associated vectors. In addition to altering the nature of the coefficients and their associated vectors, the remaining three methods implement a sample based Galerkin error minimisation technique. Table 1 summarises the proposed methods,

Table 1
Summary of the proposed methods.

Method	Form of the response vector	Coefficient	Basis	Vector of Galerkin coefficients
$M1$	$\sum_{j=1}^{n_r}\alpha_j(\omega,\theta)\mathbf{a}_j(\theta)$	$\frac{\boldsymbol{\phi}_j^T(\theta)\tilde{\mathbf{f}}_0}{\lambda_j(\theta)-\omega^2+2\mathrm{i}\sqrt{\lambda_j(\theta)}\omega\zeta}$	$\boldsymbol{\phi}_j(\theta)$	–
$M2$	$\sum_{j=1}^{n_r}\beta_j(\omega,\theta)\mathbf{b}_j$	$\frac{\boldsymbol{\phi}_{j_0}^T\tilde{\mathbf{f}}_0}{\lambda_j(\theta)-\omega^2+2\mathrm{i}\sqrt{\lambda_j(\theta)}\omega\zeta}$	$\boldsymbol{\phi}_{j_0}$	–
$M3$	$\sum_{j=1}^{N}\gamma_j(\omega)\mathbf{c}_j$	$\frac{\boldsymbol{\phi}_{j_0}^T\tilde{\mathbf{f}}_0}{\lambda_{j_0}-\omega^2+2\mathrm{i}\sqrt{\lambda_{j_0}}\omega\zeta}$	$\boldsymbol{\phi}_{j_0}$	–
$M1G$	$\sum_{j=1}^{n_r}c_j(\omega,\theta)\alpha_j(\omega,\theta)\mathbf{a}_j(\theta)$	$\frac{\boldsymbol{\phi}_j^T(\theta)\tilde{\mathbf{f}}_0}{\lambda_j(\theta)-\omega^2+2\mathrm{i}\sqrt{\lambda_j(\theta)}\omega\zeta}$	$\boldsymbol{\phi}_j(\theta)$	$\mathbf{Z}_1^{-1}(\theta,\omega)\mathbf{y}_1(\theta,\omega)$
$M2G$	$\sum_{j=1}^{n_r}c_j(\omega,\theta)\beta_j(\omega,\theta)\mathbf{b}_j$	$\frac{\boldsymbol{\phi}_{j_0}^T\tilde{\mathbf{f}}_0}{\lambda_j(\theta)-\omega^2+2\mathrm{i}\sqrt{\lambda_j(\theta)}\omega\zeta}$	$\boldsymbol{\phi}_{j_0}$	$\mathbf{Z}_2^{-1}(\theta,\omega)\mathbf{y}_2(\omega)$
$M3G$	$\sum_{j=1}^{n_r}c_j(\omega,\theta)\gamma_j(\omega)\mathbf{c}_j$	$\frac{\boldsymbol{\phi}_{j_0}^T\tilde{\mathbf{f}}_0}{\lambda_{j_0}-\omega^2+2\mathrm{i}\sqrt{\lambda_{j_0}}\omega\zeta}$	$\boldsymbol{\phi}_{j_0}$	$\mathbf{Z}_3^{-1}(\theta,\omega)\mathbf{y}_3(\omega)$

where the values of $\mathbf{Z}_1(\theta,\omega)$, $\mathbf{Z}_2(\theta,\omega)$, $\mathbf{Z}_3(\theta,\omega)$ and $\mathbf{y}_1(\theta,\omega)$, $\mathbf{y}_2(\omega)$, $\mathbf{y}_3(\omega)$ are given in Section 6. The values of $c_j(\theta,\omega)$ are subsequently located within the vectors containing the Galerkin coefficients. Thus the main difference between the $M1$, $M2$, $M3$ methods and the $M1G$, $M2G$, $M3G$ methods are the Galerkin coefficients $c_j(\theta,\omega)$. It is hoped that by computing these Galerkin coefficients the induced errors will be significantly reduced. Although the values of the Galerkin coefficients need to computed for each $\theta\in\Theta$ and $\omega\in\Omega$, this size of the linear system which needs to be solved is much lower than the size of the linear system associated with the direct Monte Carlo approach. The computational complexity associated with inversions for $\theta\in\Theta$ and $\omega\in\Omega$ are $\mathcal{O}(n_r^3)$ and $\mathcal{O}(N^3)$ respectively where $n_r<N$. In the subsequent section, the proposed methods are utilised to analyse two case systems.

9. Case studies

The six methods proposed in Sections 3 and 6 are applied to two classical structural dynamic systems. The first being an Euler–Bernoulli cantilever beam, and the second being a Kirchhoff–Love plate. Both of the analysed structures have stochastic properties. The stochastic finite element method has been applied in order to discretise both systems. Although two clamped-free systems are examined, the proposed methods can easily be utilised to analyse clamped–clamped systems. This would be executed by adapting the stochastic finite element method.

9.1. Euler–Bernoulli cantilever beam

We initially apply the proposed methods to a cantilever beam. Therefore, the displacement and rotational degrees of freedom at the clamped end of the beam are zero. The length of the beam under consideration is 1.00 m and its cross-section is a rectangle of length 0.03 m and height 0.003 m. A harmonic point load is applied at the free tip of the beam. Fig. 1 illustrates the configuration. The uncertainty is introduced through the beam's bending rigidity, EI. It is assumed that the bending rigidity is a stationary Gaussian random field of the following form

$$EI(x,\theta)=\overline{EI}(1+a(x,\theta)) \tag{79}$$

where $\overline{EI}$ denotes the deterministic value of the bending rigidity. The function $a(x,\omega)$ represents a stationary Gaussian field with zero mean, where x is the coordinate direction along the length of the beam. The covariance function is given by

$$C_a(x_1,x_2)=\sigma_a^2 e^{(|x_1-x_2|)/\mu_a} \tag{80}$$

where μ_a is the correlation length and σ_a is the standard deviation. The random field $a(x,\omega)$ can be expressed by the Karhunen–Loève expansion given by Eq. (1). The number of terms considered to represent the discretised random field is given by $M=4$.

For the deterministic case, the Young's modulus is $E=69\times10^9\ \mathrm{Nm}^{-2}$ thus corresponding to an aluminium beam. The deterministic second moment of area (moment of inertia) of the beam is $I=6.75\times10^{-11}\ \mathrm{m}^4$. Hence $\overline{EI}=4.66\ \mathrm{Nm}^2$. The correlation length μ_a is set as 0.50 m thus corresponding to half of the length of the beam. The

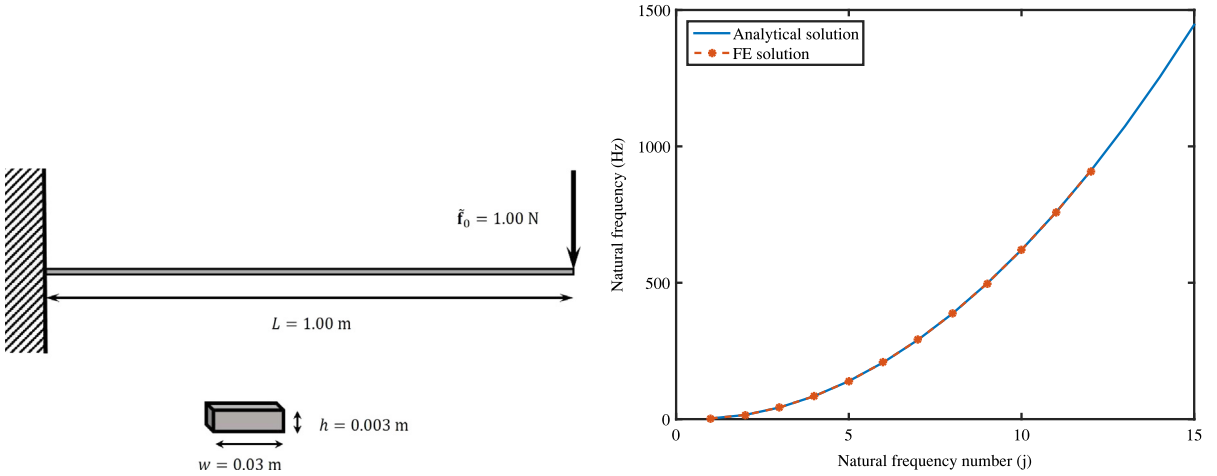

(a) The configuration of the stochastic cantilever beam with a harmonic point load asserted on the free end.

(b) Distribution of the natural frequencies of the system.

Fig. 1. A diagram of the cantilever beam system under a harmonic point load applied at the free end of the beam. The first 12 natural frequencies are depicted. These have been obtained using an analytical approach and the finite element method. It is apparent that the range of the natural frequencies covers over twice the frequency range under consideration (450 Hz).

system has been discretised into a 100 elements by using the stochastic finite element method. Consequently, after applying the appropriate boundary conditions, the dimension of the corresponding discretised system is 200×200.

The case of a unit amplitude harmonic point load acting on the free tip of the beam is considered for the frequency range 0–450 Hz at an interval of 2 Hz. This corresponds to considering 226 frequency values. For the given beam, this allows for the first eight resequence frequencies to be studied. The chosen constant modal damping model has a 2% damping factor for all the modes.

10,000 Monte Carlo simulation samples are considered for each frequency step and for two different values of the standard deviation of the bending rigidity.

$$\sigma_a = \{0.05, 0.20\}. \tag{81}$$

This allows for the methods to be compared under different levels of uncertainty. It has been numerically verified that using 10,000 Monte Carlo samples gives a satisfactory level of convergence for the first two moments of the quantities of interest.

Based on the reasoning given in Section 5, for each of the proposed methods only twelve terms have been used in the summations, hence $n_r = 12$. This is a vast reduction as 188 terms have been discarded from each method. For the deterministic case, the distribution of the natural frequencies of the cantilever beam is given in Fig. 1. The analytical natural frequencies have been computed by using the methodology given in [57] whilst the finite element solution is computed by solving Eq. (42). As to the values obtained by using the finite element method technique match the analytical values, the finite element method technique has been used for the reminder of this study. The twelve natural frequencies used in the comparison methods are highlighted in Fig. 1. As we are only considering the first twelve terms in each of the summations, the methods implementing the sample based Galerkin error minimisation technique requires a linear set of 12×12 equations to solved for each sample.

The mean vertical amplitude of the displacement at the tip of the beam is shown in Fig. 2. Barring the $M3$ method, all the projection methods seem to mimic the results obtained by using the $DMCS$ approach. The $M3$ method seems to over estimate the mean vertical amplitude at both the resonance and the antiresonance frequencies of the system. The disparity between the $M3$ and $DMCS$ methods is most prominent when $\sigma_a = 0.20$. This is due to the $M3$ method being deterministic. When the methods are stochastic, the peak responses are distributed around the corresponding resonance values. The peak responses for a deterministic system is concentrated at the resonance values, hence explaining the unsuitability of the $M3$ method in comparison with the $DMCS$ method.

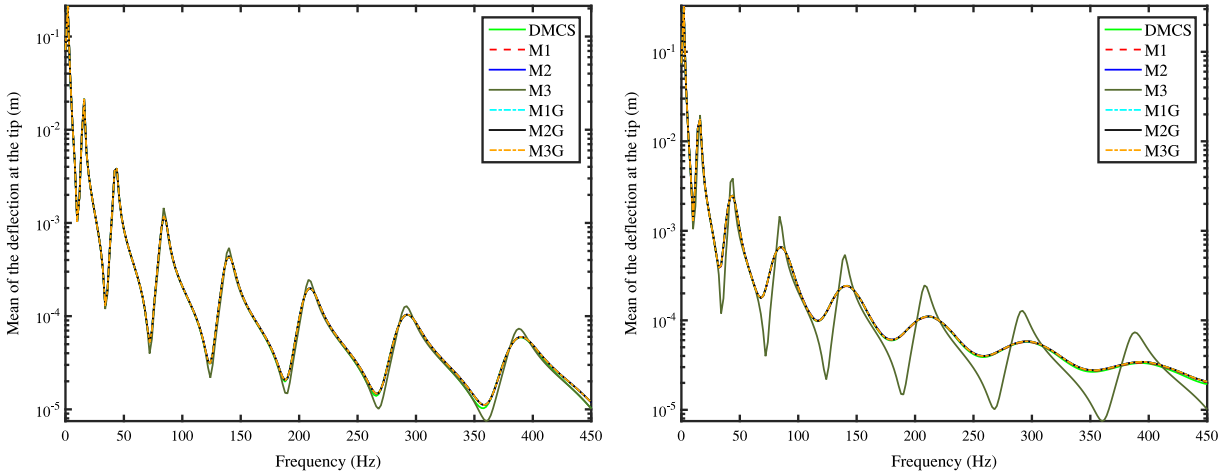

(a) $\sigma_a = 0.05$. (b) $\sigma_a = 0.20$.

Fig. 2. The mean vertical amplitude of the displacement at the tip of the beam under a unit harmonic point load at the free end. The response is shown for two different values of the standard deviation of the bending rigidity: (a) $\sigma_a = 0.05$ (b) $\sigma_a = 0.20$.

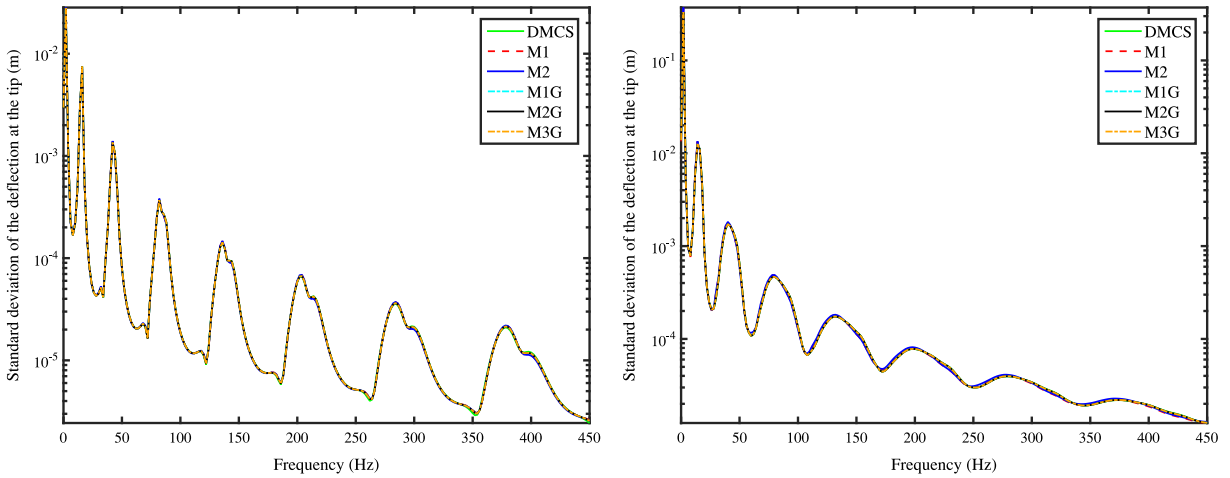

(a) $\sigma_a = 0.05$. (b) $\sigma_a = 0.20$.

Fig. 3. The standard deviation of the vertical amplitude of the displacement at the tip of the beam under a unit harmonic point load at the free end. The response is shown for two different values of the standard deviation of the bending rigidity: (a) $\sigma_a = 0.05$ (b) $\sigma_a = 0.20$.

Fig. 3 illustrates the standard deviation of the vertical amplitude of the displacement at the tip of the beam. Due to the $M3$ method being deterministic, the standard deviation associated with this method has not been illustrated. The peaks and troths of the responses seen in Fig. 3 are in agreement with those seen in Fig. 2. A decent agreement is seen between the standard deviation obtained through the $DMCS$ method and the other projection methods. However when the Galerkin error minimisation method is not implemented, a little discrepancy can be seen between the projection methods and the $DMCS$ method at high frequency values.

Fig. 4 illustrates the probability density function of the vertical amplitude at the tip of the beam. The $M3$ method has been omitted due to the lack of stochasticity. The probability density function has been computed for both values of the standard deviations at a frequency of 84 Hz. This frequency value corresponds to the fourth resonance value. All methods seem to mimic that of the $DMCS$ pretty well when $\sigma_a = 0.05$, however a disparity between the different methods is seen when $\sigma_a = 0.20$. For the higher standard deviation value, both the $M1$ and $M2$ methods do not match

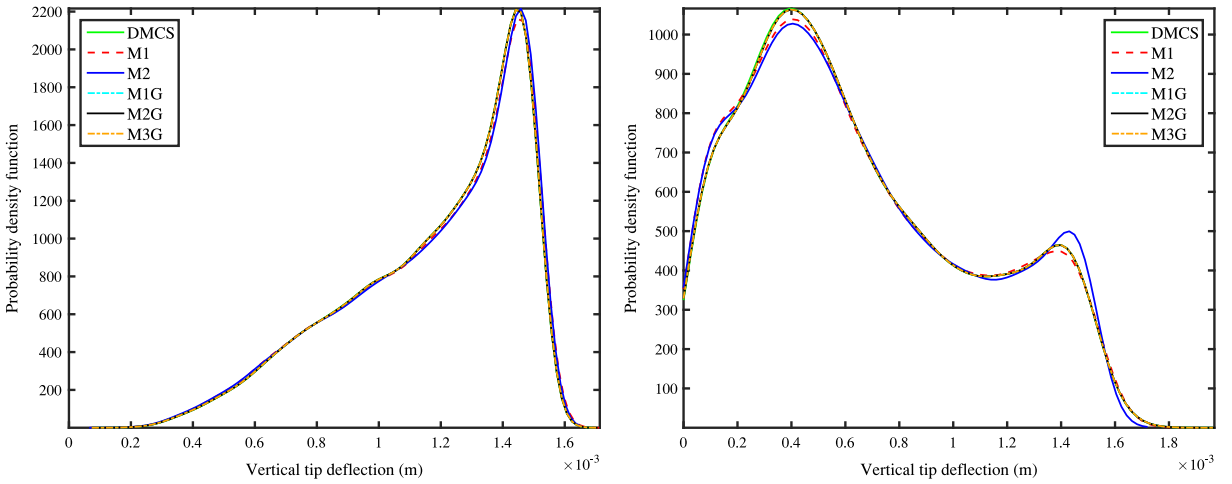

(a) $\sigma_a = 0.05$. (b) $\sigma_a = 0.20$.

Fig. 4. The probability density function of the vertical amplitude of the displacement at the tip of the beam under a unit harmonic point load at the free end at 84 Hz. The response is shown for two different values of the standard deviation of the bending rigidity: (a) $\sigma_a = 0.05$ (b) $\sigma_a = 0.20$.

the $DMCS$ method as well as the Galerkin methods. All three of the Galerkin methods seem to match the $DMCS$ method equally as well.

The approximate L_2 relative error of the mean of the response vector for each frequency step can be defined as follows

$$\hat{\varepsilon}^{\boldsymbol{\mu}}_{L_2}(\omega) = \frac{\|\boldsymbol{\mu}_{DMCS}(\omega) - \boldsymbol{\mu}_{CM}(\omega)\|_{L_2}}{\|\boldsymbol{\mu}_{DMCS}(\omega)\|_{L_2}} \tag{82}$$

where $\boldsymbol{\mu}_{DMCS}$ denotes the mean of the response vector obtained by using the $DMCS$ method and $\boldsymbol{\mu}_{CM}$ denotes the mean of the response vector obtained by using a comparable method. This method ensures that the error arising from each of the projection methods can be characterised by a single value for each $\omega \in \Omega$. Figs. 5 and 6 depict the log of the approximate L_2 relative error of the mean of the response vector for different values of n_r. This is depicted for each of the frequencies under consideration and for both values of σ_a.

It can be easily deduced that the $M3$ method introduces considerably more error than the other methods at the resonance frequencies for both values of σ_a. The visible troths seen in the relative error arising from the $M1$, $M2$, $M1G$, $M2G$ and $M3G$ methods correspond to the resonance frequencies. For a given value of n_r the trend of the approximate relative error increases with the frequency. This is to be expected as the higher order terms in the summations become more important as the frequency increases. The relative errors induced by the three sample based Galerkin methods are identical. This suggests that computing the stochastic eigensolutions is non-essential if a sample based Galerkin method is used.

The expression for the approximate L_2 relative error of the standard deviation takes a similar form

$$\hat{\varepsilon}^{\boldsymbol{\sigma}}_{L_2}(\omega) = \frac{\|\boldsymbol{\sigma}_{DMCS}(\omega) - \boldsymbol{\sigma}_{CM}(\omega)\|_{L_2}}{\|\boldsymbol{\sigma}_{DMCS}(\omega)\|_{L_2}} \tag{83}$$

where $\boldsymbol{\sigma}_{DMCS}$ denotes the standard deviation of the response vector obtained by using the $DMCS$ method and $\boldsymbol{\sigma}_{CM}$ denotes the standard deviation of the response vector obtained by using a comparable method. Figs. 7 and 8 depict the log of the approximate L_2 relative error of the standard deviation of the response vector for different values of n_r. This is depicted for both values of σ_a at each frequency step.

It is apparent that neither the $M2$ or the $M3$ methods capture the standard deviation of the $DMCS$ very well. The same is true regarding the $M1$ method, especially if the coefficient of variation is high. All three sample based Galerkin methods capture the necessary standard deviation very well, especially when the frequency value corresponds to a resonance frequency. Similarly to the case of the approximate L_2 relative error of the mean of the response vector,

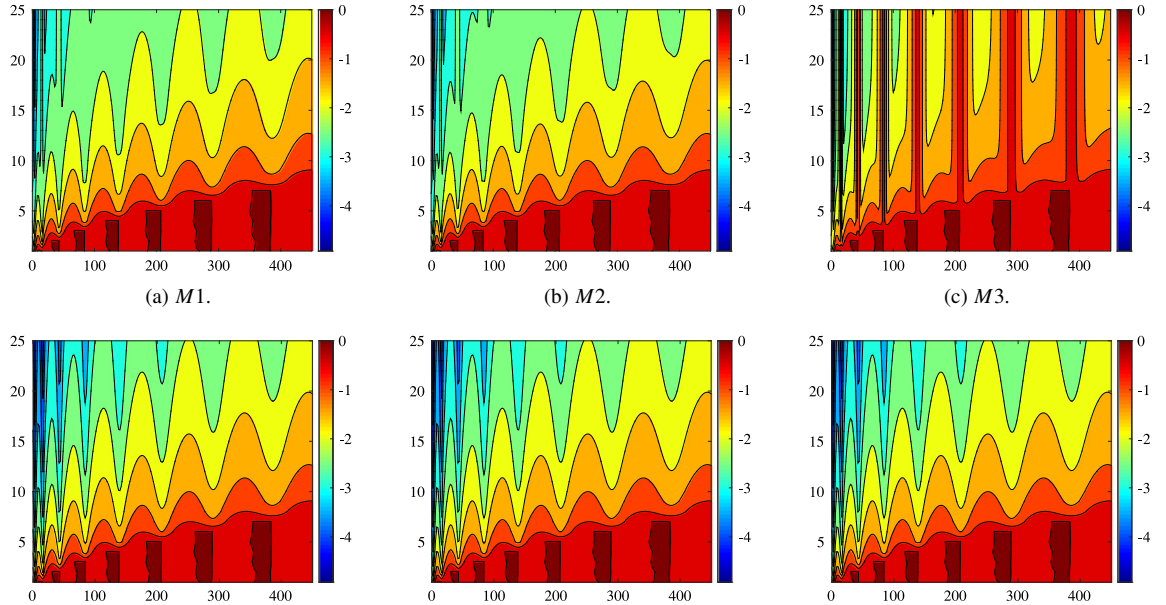

(a) $M1$. (b) $M2$. (c) $M3$.

(d) $M1G$. (e) $M2G$. (f) $M3G$.

Fig. 5. The log of the approximate L_2 relative error of the mean of the response vector when $\sigma_a = 0.05$. The contour plots depict the log of the approximate L_2 relative error for different values of n_r at each frequency step.

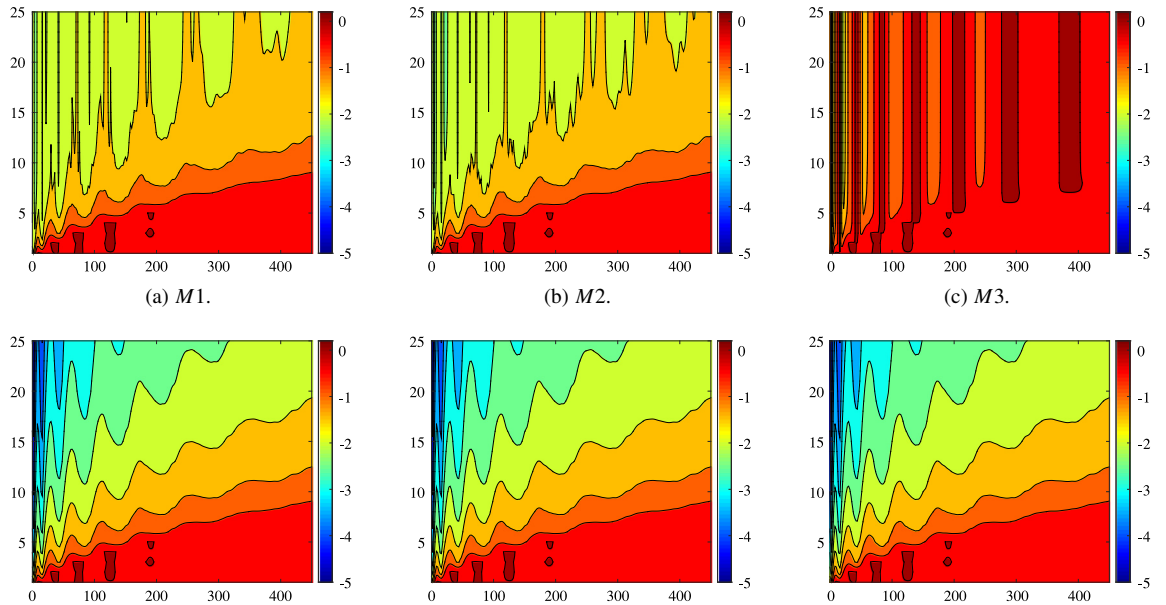

(a) $M1$. (b) $M2$. (c) $M3$.

(d) $M1G$. (e) $M2G$. (f) $M3G$.

Fig. 6. The log of the approximate L_2 relative error of the mean of the response vector when $\sigma_a = 0.20$. The contour plots depict the log of the approximate L_2 relative error for different values of n_r at each frequency step.

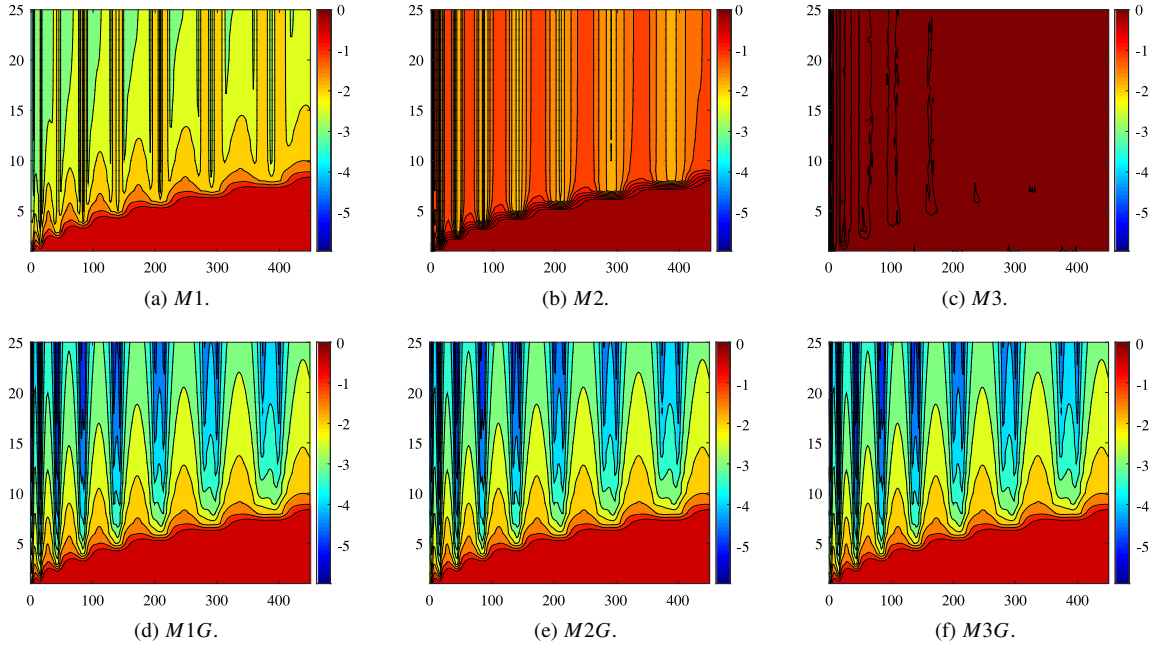

Fig. 7. The log of the approximate L_2 relative error of the standard deviation of the response vector when $\sigma_a = 0.05$. The contour plots depict the log of the approximate L_2 relative error for different values of n_r at each frequency step.

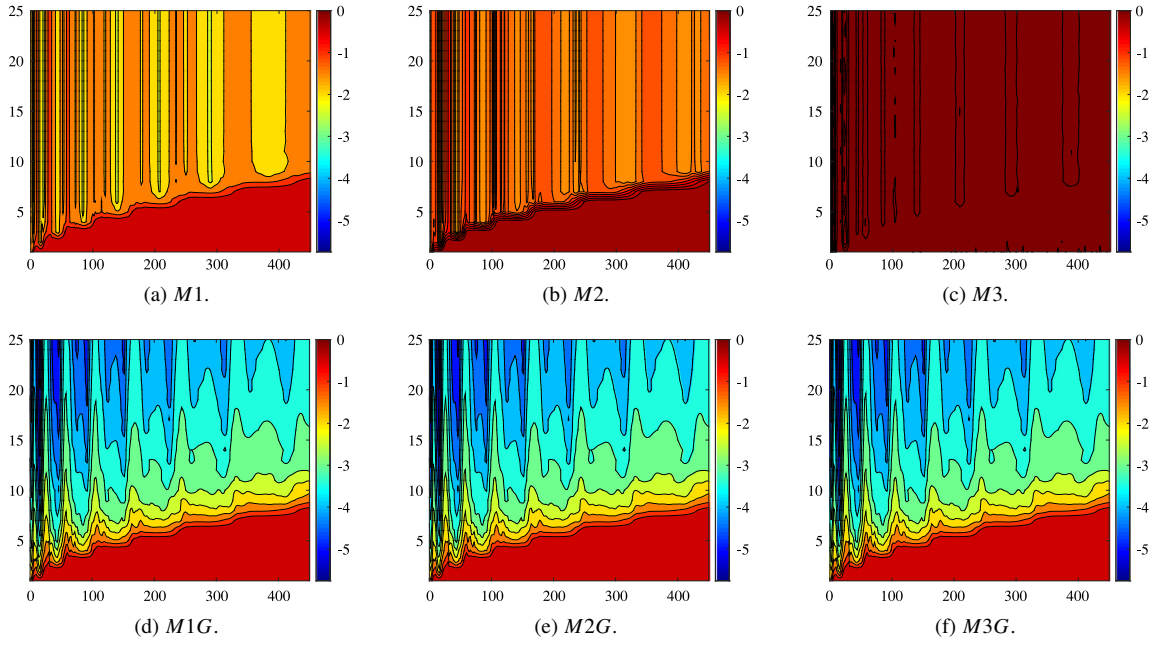

Fig. 8. The log of the L_2 relative error of the standard deviation of the response vector when $\sigma_a = 0.20$. The contour plots depict the log of the approximate L_2 relative error for different values of n_r at each frequency step.

Table 2
The approximate L_2 relative error of the mean of the response vector obtained by using the six reduced order methods for different values of n_r. The approximate L_2 relative error is shown for two different values of the standard deviation of the bending rigidity: (a) $\sigma_a = 0.05$ (b) $\sigma_a = 0.20$ at a frequency of 42 Hz.

	Number of modes	$M1$	$M2$	$M3$	$M1G$	$M2G$	$M3G$
$\sigma_a = 0.05$	6	0.0071	0.0075	0.3126	0.0064	0.0064	0.0064
	9	0.0042	0.0048	0.3136	0.0024	0.0024	0.0024
	12	0.0038	0.0044	0.3139	0.0012	0.0012	0.0012
	15	0.0037	0.0044	0.3140	0.0007	0.0007	0.0007
	18	0.0037	0.0043	0.3141	0.0004	0.0004	0.0004
$\sigma_a = 0.20$	6	0.0193	0.0197	1.7920	0.0152	0.0152	0.0152
	9	0.0159	0.0154	1.7942	0.0054	0.0054	0.0054
	12	0.0158	0.0151	1.7942	0.0027	0.0027	0.0027
	15	0.0158	0.0151	1.7949	0.0016	0.0016	0.0016
	18	0.0158	0.0151	1.7952	0.0010	0.0100	0.0010

Table 3
The approximate L_2 relative error of the standard deviation of the response vector obtained by using the six reduced order methods for different values of n_r. The approximate L_2 relative error is shown for two different values of the standard deviation of the bending rigidity: (a) $\sigma_a = 0.05$ (b) $\sigma_a = 0.20$ at a frequency of 42 Hz.

	Number of modes	$M1$	$M2$	$M3$	$M1G$	$M2G$	$M3G$
$\sigma_a = 0.05$	6	0.0149	0.0166	1.0000	0.0004	0.0004	0.0004
	9	0.0147	0.0166	1.0000	0.0001	0.0001	0.0001
	12	0.0147	0.0166	1.0000	4×10^{-5}	4×10^{-5}	4×10^{-5}
	15	0.0147	0.0166	1.0000	1×10^{-5}	1×10^{-5}	1×10^{-5}
	18	0.0147	0.0166	1.0000	1×10^{-5}	1×10^{-5}	1×10^{-5}
$\sigma_a = 0.20$	6	0.0134	0.0214	1.0000	0.0005	0.0005	0.0005
	9	0.0132	0.0213	1.0000	0.0002	0.0002	0.0002
	12	0.0132	0.0213	1.0000	0.0001	0.0001	0.0001
	15	0.0132	0.0213	1.0000	0.0001	0.0001	0.0001
	18	0.0132	0.0213	1.0000	3×10^{-5}	3×10^{-5}	3×10^{-5}

the approximate L_2 relative error of the standard deviation of the response vector are extremely similar for the three Galerkin methods under consideration.

The effect of truncating all the projection methods is further explored in Tables 2 and 3. The approximate L_2 relative error of the mean and standard deviation is explored for different values of n_r at a frequency of 42 Hz. This frequency corresponds to the third resonance value.

It is again apparent from Tables 2 and 3 that the approximate relative errors generally decrease as additional modes are introduced. It is evident that the $M3$ method is considerably worse than the other methods. The $M1$ method generally outperforms the $M2$ method, but this is to be expected due to the $M1$ method incorporating stochasticity in both the eigenvalues and eigenvectors; the stochasticity is only incorporated through the eigenvalues in the $M2$ method. All three Galerkin approaches ($M1G$, $M2G$ and $M3G$) perform equally as well, however additional computational effort is incurred whilst computing the random eigensolution associated with methods $M1G$ and $M2G$ in comparison to the $M3G$ method.

9.2. Kirchhoff–Love plate

The comparative methods are applied to analyse the bending of a thin plate which is governed by the Kirchhoff–Love plate theory. The rectangular plate under consideration has a length (L) of 1.00 m and a width (W) of 0.56 m. The centre of the plate has coordinates (0.00, 0.00). The plate is clamped along its width ($x = -0.50$ m), thus the displacement and rotational degrees of freedom along the clamped edge are zero.

Similarly to the previous case, the bending rigidity has been assumed to be the only stochastic parameter. The bending rigidity of the plate, D, is assumed to be a stationary Gaussian random field of the form

$$D(x, y, \theta) = \overline{D}(1 + a(x, y, \theta)) \tag{84}$$

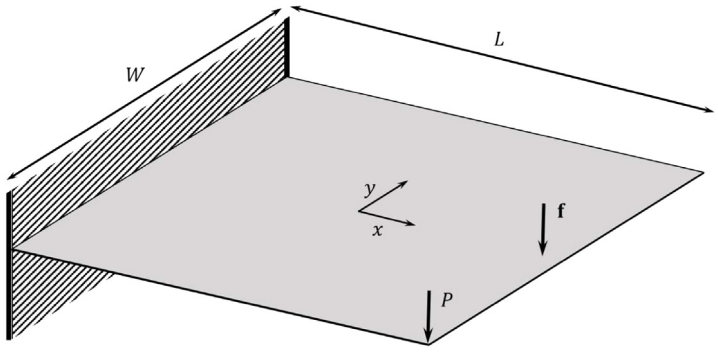

Fig. 9. The configuration of the stochastic Kirchhoff–Love plate with a harmonic point load asserted at coordinate (0.42, 0.00).

where $a(x, y, \theta)$ is a stationary Gaussian field with zero mean and x, y are the coordinate directions of the length and width of the plate. $\overline{D}$ corresponds to the deterministic value of the bending rigidity of the plate. The correlation function of the random field is assumed to take the following form

$$C_a(x_1, x_2, y_1, y_2) = \sigma_a^2 e^{-(|x_1 - x_2|)/\mu_x} e^{-(|y_1 - y_2|)/\mu_y} \tag{85}$$

where σ_a is the standard deviation of the bending rigidity, and μ_x and μ_y are the correlation lengths for both the x and y directions respectively. The forcing vector is again deemed deterministic with a unit norm. This is applied as a harmonic point load at coordinate (0.42, 0.00). The deterministic modal damping matrix consists of a 2% damping factor for each mode. Fig. 9 illustrates the configuration of the plate.

For the given example, the parameters of the plate are as follows: thickness $h = 0.003$ m, mass density $\rho = 7860$ kg m^{-3} and a Young's modulus of $E = 200 \times 10^9$ N m^{-2} thus resulting in $D_0 = 494.51$ N m. The values used imply that the thin plate is made of steel. The correlation length is set at $\mu_x = \frac{L}{5}$ i.e. a fifth of respective length in the x direction, and set at $\mu_y = \frac{W}{5}$ in the y direction.

By using a structured grid with linear rectangular elements, the thin plate has been divided into 25 elements in the x direction and 14 elements in the y direction. This leads to the system containing 1125 degrees of freedom. Three terms have been retained in the KL expansion introduced in Eq. (1) along both the x and y axis. By using a tensor product of the eigenfunctions associated with the KL expansion, a total of 9 random variables are used to represent the discretised Kirchhoff–Love plate. The response of the plate has been analysed for two different values of standard deviation

$$\sigma_a = \{0.05, 0.15\}. \tag{86}$$

The frequency range of the harmonic point load under consideration is 0–200 Hz at an interval of 2 Hz. This corresponds to considering 101 different frequency values. 5000 samples have been considered for each frequency step. 5000 samples gives a satisfactory convergence for the first two moments of the quantities of interest. For each of the proposed methods, thirty terms have been retained in their respective summations, hence $n_r = 30$. If all the terms were retained, all the summations would contain 1125 terms. The methods implementing the Galerkin error minimisation technique require a linear set of 30×30 equations to be solved for each sample.

The mean and the standard deviation of the vertical deflection amplitude of the plate is further analysed at one of the free corners $(0.50, -0.28)$. This coordinate is labelled P in Fig. 9. The mean of the vertical deflection amplitude at point P is illustrated in Fig. 10. When σ_a is set to 0.05, a good agreement between the $DMCS$ method and all the projection methods is visible. However when σ_a is increased to 0.15, an agreement between the $M3$ and $DMCS$ methods is no longer seen.

Fig. 11 shows the standard deviation of the vertical amplitude of the plate at point P. Due to the $M3$ method being deterministic, the standard deviation of this method has not been illustrated. Barring the $M2$ method, a good agreement can be seen between the $DMCS$ method and the other projection methods. Therefore it can be deemed

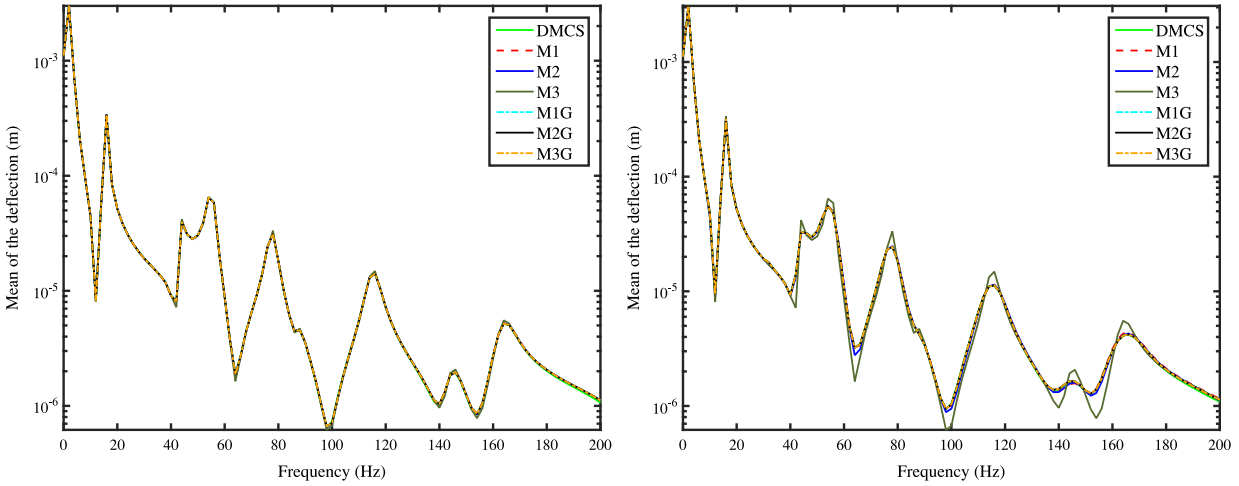

(a) $\sigma_a = 0.05$. (b) $\sigma_a = 0.15$.

Fig. 10. The mean vertical amplitude of the displacement at the corner of the plate $(0.50, -0.28)$ is observed. The response is shown for two different values of the standard deviation of the bending rigidity (a) $\sigma_a = 0.05$ (b) $\sigma_a = 0.15$.

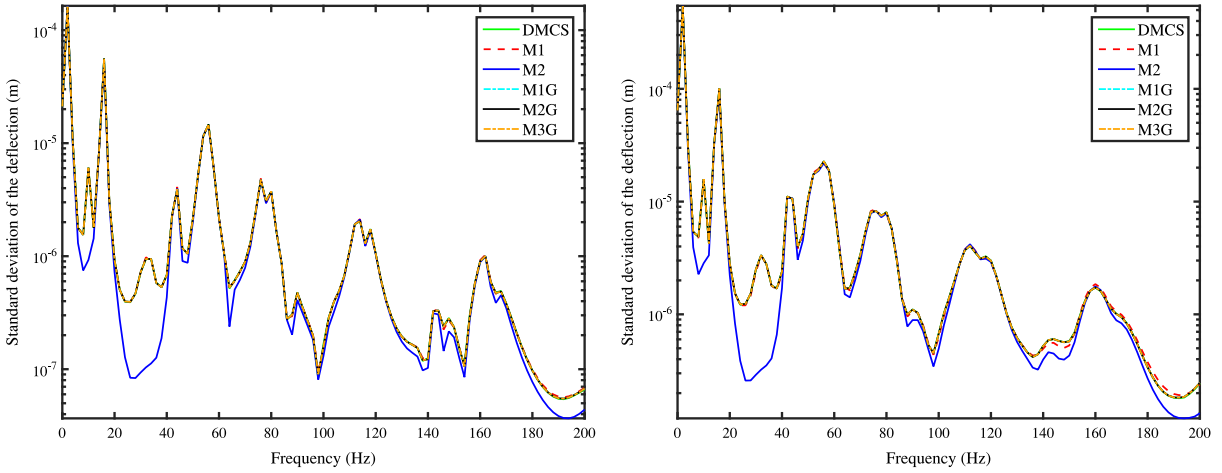

(a) $\sigma_a = 0.05$. (b) $\sigma_a = 0.15$.

Fig. 11. The standard deviation of the vertical amplitude of the displacement at the corner of the plate $(0.50, -0.28)$ is observed. The response is shown for two different values of the standard deviation of the bending rigidity (a) $\sigma_a = 0.05$ (b) $\sigma_a = 0.15$.

that only the $M1$ method or Galerkin methods can incorporate the true standard deviation of the amplitude at point P.

The approximate L_2 relative error of the mean of the response vector is given by Fig. 12 for all the proposed methods. Similarly to the cantilever beam example, the $M3$ method is extremely erroneous in comparison to the other methods. This is especially true when $\sigma_a = 0.15$. The approximate relative error seems to amplify as the frequency increases. If the value of n_r were to be increased, it is expected that the relative error at the higher frequencies would decrease. However increasing the value of n_r would increase the computational effort.

Fig. 13 depicts the approximate L_2 relative error of the standard deviation for all methods barring the $M3$ method. In conjunction with Fig. 11, it is again apparent that the $M2$ method does not capture the standard deviation of the system. It is now apparent that the $M1$ method is not as effective as the sample based Galerkin methods at mimicking the standard deviation obtained through the $DMCS$ method. By examining the sample based Galerkin methods in

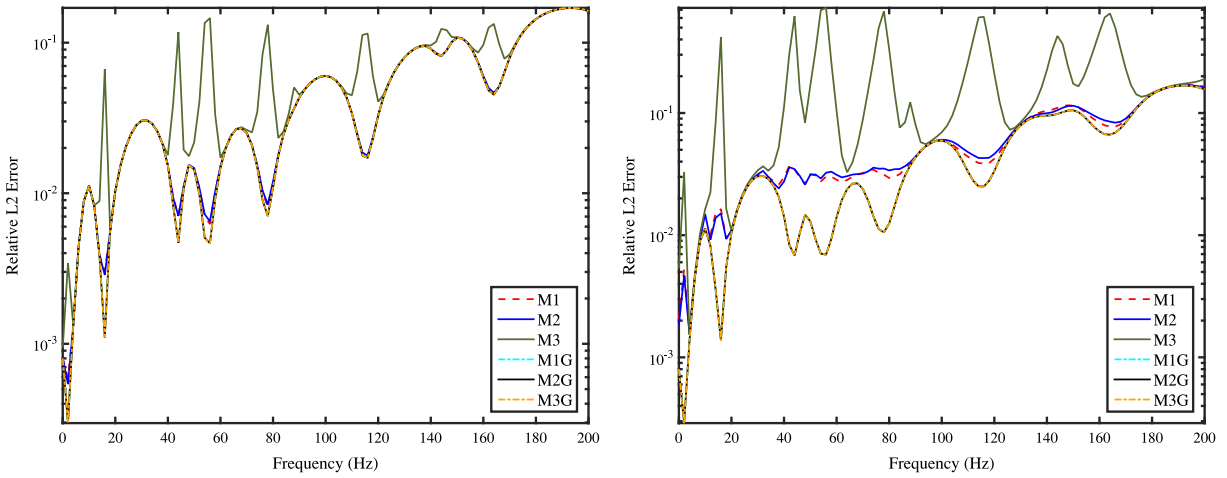

(a) $\sigma_a = 0.05$. (b) $\sigma_a = 0.15$.

Fig. 12. The approximate L_2 relative error of the mean of the response vector at each frequency step. The approximate L_2 relative error is shown for two different values of the standard deviation of the bending rigidity: (a) $\sigma_a = 0.05$ (b) $\sigma_a = 0.15$.

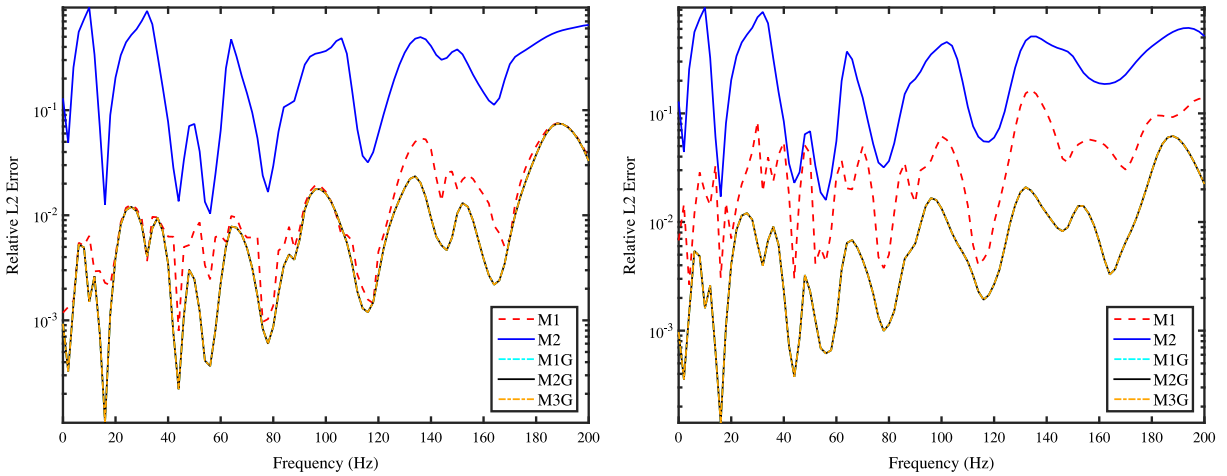

(a) $\sigma_a = 0.05$. (b) $\sigma_a = 0.15$.

Fig. 13. The approximate L_2 relative error of the standard deviation of the response vector at each frequency step. The approximate L_2 relative error is shown for two different values of the standard deviation of the bending rigidity: (a) $\sigma_a = 0.05$ (b) $\sigma_a = 0.15$.

more detail, all the methods produce an extremely similar value of relative error. This is the case for both the relative error of the mean and the standard deviation. Therefore it can be deduced that calculating or approximating the random eigensolutions is not necessary in order to obtain the lowest relative errors for the mean and standard deviation. Combining deterministic eigensolutions and the sample based Galerkin approach is sufficient.

The probability density function of the vertical amplitude of the point P is given in Fig. 14. This has been calculated for both values of σ_a at 168 Hz. This frequency value corresponds to the 16th deterministic resonance value. Due to the deterministic nature of the $M3$ method, its probability density function has been omitted. A decent agreement can be seen between all the methods at the lower σ_a value, however a greater discrepancy is seen between the methods at the largest value of σ_a. When $\sigma_a = 0.15$ a good agreement is seen between the Galerkin methods and the $DMCS$ method, however the $M1$ and $M2$ methods are less successful at mimicking the probability density function of the $DMCS$ method.

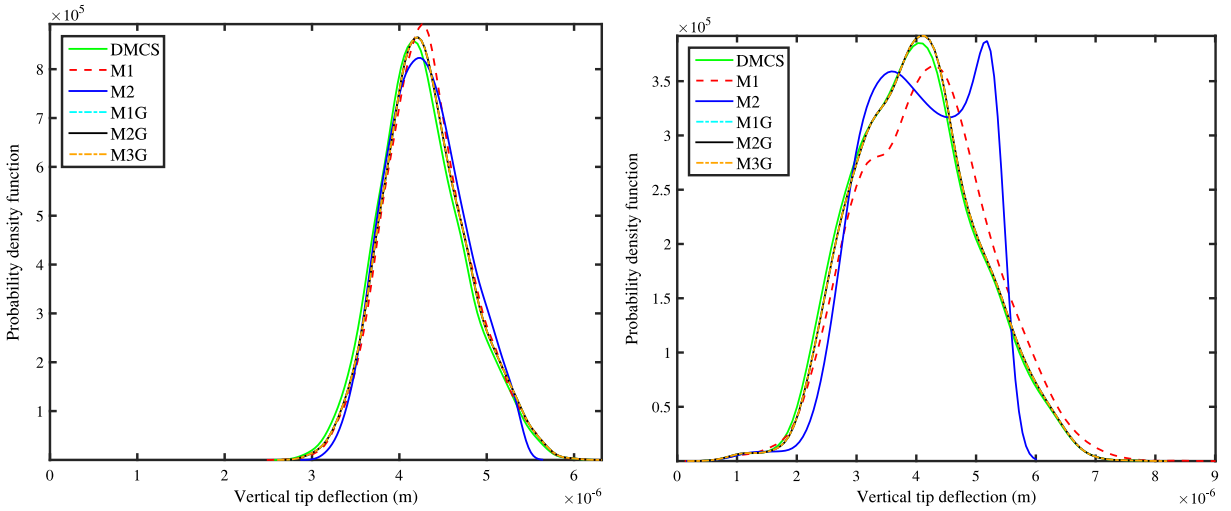

Fig. 14. The probability density function of the vertical amplitude of the displacement at the corner of the plate (0.50, −0.28) when the unit harmonic point load at (0.42, 0.00) is at 168 Hz. The response is shown for two different values of the standard deviation of the bending rigidity: (a) $\sigma_a = 0.05$ (b) $\sigma_a = 0.15$.

10. Summary and conclusion

10.1. Summary

A summary of the proposed methods is given below:

- A set of hybrid projection methods to calculate the response of stochastic dynamic structural systems has been proposed. The different methods analyse the effect of altering the nature of the coefficients and their associated basis.
- Both the coefficients and their corresponding basis have been computed by utilising the stochastic and deterministic eigensolutions of the structural system.
- The computational effort is reduced by approximating the stochastic eigensolutions and by reducing the modal basis.
- To compensate for the error induced by the proposed hybrid model order reduction technique, a sample based Galerkin error minimisation approach is presented.
- If the sample based Galerkin error minimisation approach is omitted it is necessary for both the coefficients and their associated bases to be stochastic in order to capture an accurate response for a system.
- If the Galerkin error minimisation approach is applied calculating the stochastic eigensolutions is unwarranted. The Galerkin method compensates for the error induced while utilising the baseline eigenmodes. Therefore, a Monte Carlo type sample-based method to evaluate the coefficients and their associate basis can be avoided.
- The application of the Galerkin error minimisation approach in conjunction with projecting onto a deterministic basis with deterministic coefficients ($M3G$) produces a level of accuracy comparable to any of the other proposed methods. Our study leads us to suggest that this simple approach has significant potential for analysing stochastic structural systems.

10.2. Conclusion

A comprehensive set of hybrid projection methods has been proposed in order to solve a stochastic partial differential equation for structural dynamic systems. Following the implementation of a stochastic finite element

method, three projection methods have been developed by utilising the random eigenvalue problem. The first method utilises both random eigenvalues and eigenvectors, the second random eigenvalues and deterministic eigenvectors and the third only uses deterministic eigensolutions. In order to reduce the computational effort associated with each of these methods, the random eigensolutions have been approximated by a first order perturbation and only the dominant projection terms have been retained. Due to the approximations and the reduced modal basis, three additional projection methods have been proposed. These methods utilise a sample based Galerkin error minimisation approach in order to lower the error.

The proposed methods have been applied to a Euler–Bernoulli cantilever beam and to a Kirchhoff–Love plate with stochastic properties described with a random field. It is apparent that if the sample based Galerkin error minimisation approach were not to be implemented the stochastic elastic properties of the random eigenvalues and eigenvectors must be retained in order to capture the stochasticity of the governing equation. The application of the sample based Galerkin method compensates the error incurred when only the baseline eigenmodes are utilised. Thus the significant computational overhead associated with a Monte Carlo type sample-based basis evaluation is avoided when using the proposed Galerkin error minimisation technique. Future research needs to verify these conclusions for larger real-life structures and different models of uncertainties. One of the main difficulties that needs to be addressed is the elicitation of uncertainties in stochastic parameters for real-life structures. This might require complex hierarchical probabilistic uncertainty descriptors which then must be translated into parametrised coefficient matrices. Additionally, the consideration of non-proportional damping matrices and projection in the space of complex eigenmodes [52] will be a fruitful generalisation of the proposed framework.

Acknowledgements

The authors acknowledge the financial support received from Engineering Research Network Wales (one of three Sêr Cymru National Research Networks) with Grant Numbers NRN125 and NRNC25.

References

[1] J.E. Hurtado, A.H. Barbat, Monte carlo techniques in computational stochastic mechanics, Arch. Comput. Methods Eng. 5 (1) (1998) 3–29.
[2] R.C. Smith, Uncertainty Quantification : Theory, Implementation, and Applications, SIAM, 2014.
[3] V.J. Romero, J.V. Burkardt, M.D. Gunzburger, J.S. Peterson, Comparison of pure and “latinized” centroidal voronoi tessellation against various other statistical sampling methods, Reliab. Eng. Syst. Saf. 91 (10–11) (2006) 1266–1280.
[4] I.G. Graham, F.Y. Kuo, J.A. Nichols, R. Scheichl, C. Schwab, I.H. Sloan, Quasi-monte carlo finite element methods for elliptic pdes with lognormal random coefficients, Numer. Math. 131 (2) (2015) 329–368.
[5] J. Dick, F.Y. Kuo, I.H. Sloan, J. Dick, F.Y. Kuo, I.H. Sloan, High-dimensional integration: The quasi-Monte Carlo way, Acta Numer. (2013) 133–288.
[6] J.C. Helton, F.J. Davis, Latin hypercube sampling and the propagation of uncertainty in analyses of complex systems, Reliab. Eng. Syst. Saf. 81 (1) (2003) 23–69.
[7] M. Kim, I. Sim, Projected Multilevel Monte Carlo Method for PDE with random input data, eprint arXiv:1502.07486.
[8] P. Hauseux, J.S. Hale, S.P.A. Bordas, Accelerating Monte Carlo estimation with derivatives of high-level finite element models, Comput. Methods Appl. Mech. Engrg. 318 (2017) 917–936.
[9] S.K. Au, J.L. Beck, Subset simulation and its application to seismic risk based on dynamic analysis, J. Eng. Mech. 129 (8) (2003) 901–917.
[10] F. Wu, Q. Gao, X.-M. Xu, W.-X. Zhong, F. Wu, Q. Gao, X.-M. Xu, W.-X. Zhong, A modified computational scheme for the stochastic perturbation finite element method, Lat. Am. J. Solids Struct. 12 (13) (2015) 2480–2505.
[11] O. Cavdar, A. Bayraktar, A. Cavdar, S. Adanur, Perturbation based stochastic finite element analysis of the structural systems with composite sections under earthquake forces, Steel Compos. Struct. 8 (2) (2008) 129–144.
[12] D. Sarsri, L. Azra, Dynamic analysis of large structures with uncertain parameters based on coupling component mode synthesis and perturbation method, Ain Shams Eng. J. 7 (1) (2016) 371–381.
[13] G. Falsone, N. Impollonia, A new approach for the stochastic analysis of finite element modelled structures with uncertain parameters, Comput. Methods Appl. Mech. Engrg. 191 (44) (2002) 5067–5085.
[14] G. Falsone, G. Ferro, An exact solution for the static and dynamic analysis of FE discretized uncertain structures, Comput. Methods Appl. Mech. Engrg. 196 (21–24) (2007) 2390–2400.
[15] D. Settineri, G. Falsone, An APDM-based method for the analysis of systems with uncertainties, Comput. Methods Appl. Mech. Engrg. 278 (2014) 828–852.
[16] F. Yamazaki, M. Shinozuka, G. Dasgupta, Neumann expansion for stochastic finite-element analysis, J. Eng. Mech.-Asc 114 (8) (1988) 1335–1354.
[17] S. Adhikari, C.S. Manohar, Dynamic analysis of framed structures with statistical uncertainties, Internat. J. Numer. Methods Engrg. 44 (1999) 1157–1178.

[18] X. Wang, S. Cen, C. Li, Generalized Neumann expansion and its application in stochastic finite element methods, Math. Probl. Eng. 2013 (2013) 1–13.
[19] H.-R. Bae, R.V. Grandhi, R.A. Canfield, Successive matrix inversion method for reanalysis of engineering structural systems, AIAA J. 42 (8) (2004) 1529–1535.
[20] H.-R. Bae, E.E. Forster, Improved Neumann expansion method for stochastic finite element analysis, J. Aircr. 54 (3) (2017) 967–979.
[21] N. Wiener, The homogeneous chaos, Amer. J. Math. 60 (4) (1938) 897–936.
[22] R.G. Ghanem, P.D. Spanos, Stochastic Finite Elements: A Spectral Approach, revised ed., Dover Publications Inc., 2012.
[23] D.B. Xiu, G.E. Karniadakis, The wiener-askey polynomial chaos for stochastic differential equations, SIAM J. Sci. Comput. 24 (2) (2002) 619–644.
[24] D.B. Xiu, G.E. Karniadakis, Modeling uncertainty in flow simulations via generalized polynomial chaos, J. Comput. Phys. 187 (1) (2003) 137–167.
[25] A. Kundu, S. Adhikari, Dynamic analysis of stochastic structural systems using frequency adaptive spectral functions, Probab. Eng. Mech. 39 (2015) 23–38.
[26] F. André, A polynomial chaos approach to narrow band modeling of radiative heat transfer in non-uniform gaseous media, J. Quant. Spectrosc. Radiat. Transfer 175 (2016) 17–29.
[27] L. Parussini, V. Pediroda, C. Poloni, Prediction of geometric uncertainty effects on fluid dynamics by polynomial chaos and fictitious domain method, Comput. & Fluids 39 (1) (2010) 137–151.
[28] E. Jacquelin, S. Adhikari, J.-J. Sinou, M.I. Friswell, Polynomial chaos expansion in structural dynamics: Accelerating the convergence of the first two statistical moment sequences, J. Sound Vib. 356 (2015) 144–154.
[29] S. Wu, S. Law, A reduced polynomial chaos expansion model for stochastic analysis of a moving load on beam system with non-Gaussian parameters, J. Vibroeng. 17 (3) (2015) 1560–1577.
[30] V. Yaghoubi, S. Marelli, B. Sudret, T. Abrahamsson, Sparse polynomial chaos expansions of frequency response functions using stochastic frequency transformation, Probab. Eng. Mech. 48 (2017) 39–58.
[31] R. Schöbi, B. Sudret, Uncertainty propagation of p-boxes using sparse polynomial chaos expansions, J. Comput. Phys. 339 (2017) 307–327.
[32] S. Abraham, M. Raisee, G. Ghorbaniasl, F. Contino, C. Lacor, A robust and efficient stepwise regression method for building sparse polynomial chaos expansions, J. Comput. Phys. 332 (2017) 461–474.
[33] J. Hampton, A. Doostan, Compressive sampling of polynomial chaos expansions: Convergence analysis and sampling strategies, J. Comput. Phys. 280 (2015) 363–386.
[34] G. Migliorati, F. Nobile, E. von Schwerin, R. Tempone, Approximation of quantities of interest in stochastic PDEs by the random discrete l^2 projection on polynomial spaces, SIAM J. Sci. Comput. 35 (3) (2013) A1440–A1460.
[35] T. Kim, Frequency-domain karhunen–loeve method and its application to linear dynamic systems, AIAA J. 36 (11) (1998) 2117–2123.
[36] K. Kunisch, S. Volkwein, Optimal snapshot location for computing POD basis functions, ESAIM Math. Model. Numer. Anal. 44 (3) (2010) 509–529.
[37] K. Willcox, J. Peraire, Balanced model reduction via the proper orthogonal decomposition, AIAA J. 40 (11) (2002).
[38] J.S. Hesthaven, G. Rozza, B. Stamm, Certified Reduced Basis Methods for Parametrized Partial Differential Equations, in: SpringerBriefs in Mathematics, Springer International Publishing, Cham, 2016.
[39] A. Quarteroni, A. Manzoni, F. Negri, Reduced Basis Methods for Partial Differential Equations, Vol. 92, Springer International Publishing, Cham, 2016.
[40] A. Quarteroni, G. Rozza, Reduced Order Methods for Modeling and Computational Reduction, Springer International Publishing, 2014.
[41] P. Benner, S. Gugercin, K. Willcox, A survey of projection-based model reduction methods for parametric dynamical systems, SIAM Rev. 57 (4) (2015) 483–531.
[42] K. Serafin, B. Magnain, E. Florentin, N. Parés, P. Díez, Enhanced goal-oriented error assessment and computational strategies in adaptive reduced basis solver for stochastic problems, Internat. J. Numer. Methods Engrg. 110 (5) (2017) 440–466.
[43] E. Florentin, P. Díez, Adaptive reduced basis strategy based on goal oriented error assessment for stochastic problems, Comput. Methods Appl. Mech. Engrg. 225–228 (2012) 116–127.
[44] A. Sofi, E. Romeo, A unified response surface framework for the interval and stochastic finite element analysis of structures with uncertain parameters, Probab. Eng. Mech. (2017).
[45] Z. Zhang, C. Jiang, D. Han, X. amd Hu, S. Yu, A response surface approach for structural reliability analysis using evidence theory, Adv. Eng. Softw. 69 (2014) 37–45.
[46] X. Zhai, C.-W. Fei, Y.-S. Choy, J.-J. Wang, A stochastic model updating strategy-based improved response surface model and advanced Monte Carlo simulation, Mech. Syst. Signal Process. 82 (2017) 323–338.
[47] G. Stefanou, The stochastic finite element method: Past, present and future, Comput. Methods Appl. Mech. Engrg. 198 (9–12) (2009) 1031–1051.
[48] A. Nouy, Recent developments in spectral stochastic methods for the numerical solution of stochastic partial differential equations, Arch. Comput. Methods Eng. 16 (2009) 251–285.
[49] S. Daouk, F. Louf, O. Dorival, L. Champaney, S. Audebert, Uncertainties in structural dynamics: overview and comparative analysis of methods, Mech. Ind. 16 (4) (2015) 404.
[50] S.E. Pryse, S. Adhikari, Stochastic finite element response analysis using random eigenfunction expansion, Comput. Struct. 192 (2017) 1–15.
[51] S.E. Pryse, S. Adhikari, A. Kundu, Sample-based and sample-aggregated based Galerkin projection schemes for structural dynamics, Probab. Eng. Mech. (2017). http://dx.doi.org/10.1016/j.probengmech.2017.09.002.
[52] S. Adhikari, Structural Dynamic Analysis with Generalized Damping Models: Analysis, Wiley ISTE, UK, 2013.

[53] D. Charmpis, G. Schuëller, M. Pellissetti, The need for linking micromechanics of materials with stochastic finite elements: A challenge for materials science, Comput. Mater. Sci. 41 (1) (2007) 27–37.
[54] M. Ainsworth, J. Oden, A posteriori error estimation in finite element analysis, Comput. Methods Appl. Mech. Engrg. 142 (1–2) (1997) 1–88.
[55] R.L. Fox, M.P. Kapoor, Rates of change of eigenvalues and eigenvectors, AIAA J. 6 (12) (1968) 2426–2429.
[56] M.I. Friswell, The derivatives of repeated eigenvalues and their associated eigenvectors, J. Vib. Acoust. 118 (3) (1996) 390.
[57] M. Geradin, D. Rixen, Mechanical Vibrations: Theory and Application to Structural Dynamics, third ed., John Wiley, 2015.